Page curves in holographic superconductors

Yuanceng Xu,[1,*] Dong Wang,[2,†] and Qiyuan Pan[3,‡]

[1]*Institute of Astrophysics, Central China Normal University, Wuhan, Hubei 430079, China*
[2]*School of Sciences, Hunan University of Technology, Zhuzhou, Hunan 412008, China*
[3]*Key Laboratory of Low Dimensional Quantum Structures and Quantum Control of Ministry of Education, Synergetic Innovation Center for Quantum Effects and Applications, and Department of Physics, Hunan Normal University, Changsha, Hunan 410081, China*

(Received 17 January 2024; accepted 3 July 2024; published 5 August 2024)

Considering a doubly holographic model, we study the black hole information paradox for the eternal AdS$_d$-RN black hole coupled to and in equilibrium with a d-dimensional conformal bath whose state has been deformed by the charged scalar field coupled to a U(1) gauge field. Without a brane, the spontaneous symmetry breaking of the gauge field on boundary systems can induce a second-order phase transition of the charged scalar field at the critical temperature, known as holographic superconductors. The bath deformation can significantly change its entanglement dynamics with the black hole, resulting in variations in the Page curve and Page time. Our results indicate that characteristic parameters of the Page curve, such as entanglement velocity, initial area difference and Page time, can be used as suitable probes to detect superconducting phase transitions. In particular, the entanglement velocity can also probe both Kasner flows and Josephson oscillations. When keeping the endpoint of the radiation region fixed at twice the critical Page point, the entanglement velocity (the internal backreaction) has a more significant influence on the Page time compared to the initial area difference (the external backreaction).

DOI: 10.1103/PhysRevD.110.046003

I. INTRODUCTION

A recent study on the black hole information paradox confirms that information within a black hole can be extracted through Hawking radiation, preserving the information conservation and the quantum-mechanical unitarity [1–4] (see, e.g., [5] for a review). Unlike previous calculations by Hawking [6], the novel research approach focuses on the computation of the fine-grained entropy of the late-time "radiation" region $\mathcal{R}$, emphasizing the need to simultaneously consider the fine-grained entropy of an interior region within the black hole, referred to as the "island" $\mathcal{I}$ whose boundary corresponds to a "quantum extreme surface" (QES) [7] $\partial\mathcal{I}$.

$$S(R) = \min\left\{\operatorname{ext}\left[\frac{\operatorname{Area}(\partial\mathcal{I})}{4G_N} + S_{\text{matter}}(\mathcal{I}\cup\mathcal{R})\right]\right\}. \quad (1)$$

[1] Due to the entanglement between antiparticles within the island and outward-radiating positive particles, when considering the entanglement entropy of both regions together, particle-antiparticle pairs cancel each other out, resulting in a total entanglement entropy smaller than that of the isolated radiation region. This alignment with the Page curve [8,9] demonstrates that the Hawking radiation maintains unitarity, affirming the conservation of the black hole information.

Early investigations into the island rule primarily centered around two-dimensional dilaton gravity models. Because the two-dimensional gravity allows for replica wormholes [10,11], enabling a more rigorous derivation of the island formula. Subsequently, the island rule was extended to higher-dimensional scenarios through the use of doubly holographic models [4,12]: the d-dimensional anti-de Sitter (AdS$_d$) gravity theory coupled to the matter [conformal field theory (CFT$_d$)] that has a $(d+1)$-dimensional

*Contact author: xyc@mails.ccnu.edu.cn
†Contact author: indulge_chen@163.com
‡Contact author: panqiyuan@hunnu.edu.cn

[1]The different calligraphic styles between the symbol "R" on the left-hand side and the symbol "$\mathcal{R}$" on the right-hand side in Eq. (1) may cause confusion, hence clarification is required. the symbol "R" on the left-hand side we mean the radiation in the full quantum description. The full entropy of radiation $S(R)$ can be computed using the gravitational fine-grained entropy formula. In contrast, the symbol "$\mathcal{R}$" on the right-hand side we mean the description of radiation *in the semiclassical description* [3,5].

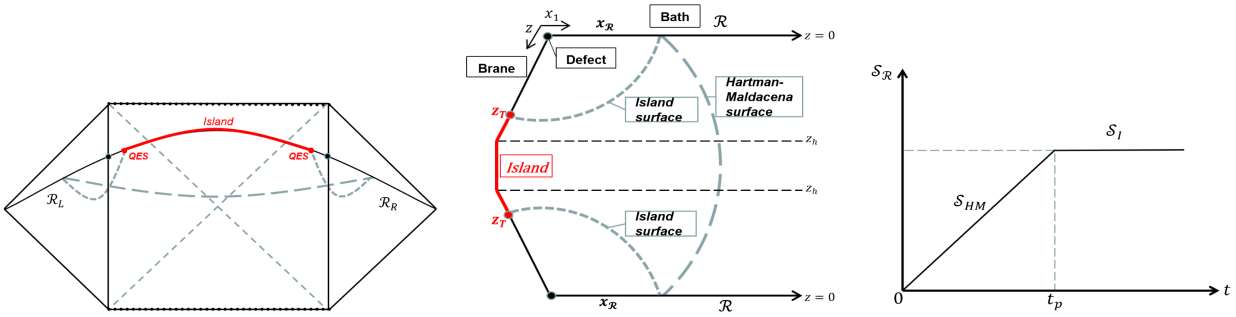

FIG. 1. (a) The eternal two-side black hole and the island that emerges after Page time with QES outside the horizon. (b) Two different candidate RT minimal surfaces in a doubly holographic setup. (c) The early part of the Page curve is determined by the time-dependent HM surface, while the later part of the Page curve is determined by the constant island surface. The Page curve *generally does not* saturate to $2S_{\mathrm{BH}}$ in the doubly holographic setup.

holographic dual, which is a higher-dimensional version of the Randall-Sundrum (RS) setup [13,14]. The AdS_d-Einstein gravity coupled with the CFT_d-matter is referred to as the RS brane or Planck brane. It is termed "double holography" because it leverages two instances of the AdS/CFT holographic duality, thus establishing connections among three equivalent descriptions for the same system [15–44]:

(I) Boundary perspective: A d-dimensional boundary conformal field theory (BCFT_d) with a $(d-1)$-dimensional boundary.
(II) Bulk perspective: An asymptotically AdS_{d+1} Einstein gravity with an AdS_d RS brane.
(III) Brane perspective: A CFT_d living on the AdS_d brane with a boundary CFT_d bath in the flat space linked by transparent boundary conditions.

The description (III) precisely simulates the Hawking radiation process of a black hole. The advantage of double holography is that the entanglement dynamics between the black hole and radiation region are reflected instantaneously in the corresponding entanglement wedges (EW) in the bulk of description (II). Then, according to the Ryu-Takayanagi/Hubeny-Rangamani-Takayanagi (RT/HRT) formula [45,46], by replacing the computation of QES's areas with the computation of RT/HRT surface's areas in the bulk of the description (II) at different times, we can obtain the entanglement entropy of the CFT in the black hole and radiation region at different stages of the radiation. Specifically, we consider a two-sided black hole coupled to two flat baths, one on each side. More precisely, we fix one end of the RT surface at the conformal boundary at a given location $x_{\mathcal{R}}$. As we extend from $x_{\mathcal{R}}$ into the bulk, there are two candidate RT surfaces of interest. One is the extremal surface whose endpoint terminates on the brane, called the "island surface." The other is the extremal surface that passes through the black hole event horizon, reaches a radial critical point z_* inside the black hole, and then exits the horizon to reach another boundary, known as the "Hartman-Maldacena (HM) surface" [47]. In other words, with the doubly holographic setup, the entanglement entropy of radiation can be simply evaluated using the following formula

$$S(R) = \min_{\mathcal{I}} \left[\frac{\mathrm{Area}(\gamma_{\mathcal{I}\cup\mathcal{R}})}{4G_N^{(d+1)}} \right], \tag{2}$$

where $\gamma_{\mathcal{I}\cup\mathcal{R}}$ is the standard codimension two HRT surface in the bulk, corresponding to the HM surface (γ_{HM}) or island surface (γ_I). Two candidate extremal surfaces in the doubly holographic model are presented in Fig. 1(b). Because the Einstein-Rosen (ER) bridge grows with time, the area of the HM surfaces increases from the initial time ($t = 0$). On the other hand, the area of the island surface is time-independent, making it a constant. Figure 1(c) is the time-evolution curve of the radiation region's entanglement entropy, known as the Page curve. It is worth noting that when using the doubly holographic setup, the entanglement entropy of the radiation for an eternal black hole *generally does not* saturate to twice the Bekenstein-Hawking entropy S_{BH} [12,21],[2] which exhibits noticeable differences from the analytical results obtained using the s-wave approximation [3,48–60]. The initial part of the Page curve, which increases with time, is obtained by calculating the area of time-dependent HM surfaces. The latter part of the Page curve, which is independent of time, is obtained by calculating the area of island surfaces. To obtain a reasonable Page curve, the area of the HM surface at the initial time ($t = 0$) must be smaller than the area of the island surface. Thus, the endpoint $x_{\mathcal{R}}$ of the radiation region must be larger than the "Page point" x_p, which is the value of $x_{\mathcal{R}}$ when the initial HM surface's area is equal to that of the island surface. Both candidate extremal surfaces diverge at the UV conformal boundary, so the standard holographic renormalization will be

[2]It should be emphasized that the authors of [40] claim to have provided the first-ever demonstration that, even when considering the doubly holographic setup, the saturated value of entanglement entropy after the Page time can be comparable to twice the Bekenstein-Hawking entropy.

used to remove these divergent terms using a cutoff ($\epsilon = z/z_h \ll 1$) at the boundary.

Description III primarily discusses the coupling of a RS brane and a nongravitating bath on the conformal boundary with transport boundary conditions at their intersection (i.e., the defect). Due to conformal baths and transport boundary conditions, the gravity on the brane becomes massive [17]. This raises a fundamental question: is it necessary, in our physical reality, for gravitons to have mass to address the black hole information paradox? In other words, do we require such a bath for a comprehensive understanding of our Universe? In fact, the bath imposes too many computational constraints. To investigate to how the presence of the bath affects the explanation of the black hole information paradox, the author of [29] introduces a scalar operator ϕ as a new, tunable scale to deform the bath, allowing us to explore how different degrees of bath deformation influence the Page curve. The deformation triggers a holographic RG flow [61–64]. A significant conclusions in [29] is that the Page curve can serve as a probe for the holographic RG flow. We hope to extend the research presented in [29] further. Specifically, we intend to deform the bath using a charged scalar field, which involves coupling the charged scalar field with a U(1) gauge field. The U(1) symmetry is broken by the gauge field, inducing a second-order phase transition of the charged scalar field at the critical temperature, known as holographic superconductors [65–67]. Motivated by the exploration of utilizing entanglement entropy as a good probe for detecting holographic superconducting phase transitions, such as s-wave [68–77], p-wave [78–82], d-wave [83] metal/superconductor phase transitions, and s-wave [84–90], p-wave [91] insulator/superconductor phase transitions, this article aims to explore, within the context of the doubly holographic setup, not only whether the Page curve can probe the Kasner flows, but more importantly, whether the Page curve and Page time can track the information of the superconducting phase transition.

It should be noted that when considering tensionless branes and using the RT formula to calculate the entanglement entropy of the radiation, the correction due to quantum fluctuations of the CFT on the brane is highly important and non-negligible. Thus, in the double-holographic literature, the tension is commonly taken to be very large. Only in this limit, the entanglement entropy computed with the higher dimensional RT prescription coincides with the entanglement entropy computed using the island formula in the induced theory on the brane, which has been pointed out in Refs. [36,50]. Fortunately, just as in Ref. [17], we still consider removing half of the space and calculating the entanglement entropy by using the RT formula for the tensionless limit.[3] Actually, there are many other papers about the double holography or the AdS/BCFT with tensionless branes, for examples [20,21,29,32,35,40,92–101]. Nevertheless, the results of our paper can be used to provide a qualitative picture of the Page curve.

Similar to the neutral case [102,103], with no branes, introducing a charged scalar field on the conformal boundary transforms the geometry near the singularity of the AdS-Reissner-Nordström (AdS-RN) black hole into a Kasner universe. Furthermore, it is noteworthy that the charged scalar hair brings about significant changes in the dynamical structure inside the AdS-RN black hole. Specifically, the black hole's interior dynamics are cleanly separated into three different epochs [104,105]: the collapse of ER bridge, Joseph oscillations and Kasner universe; in some cases, it even undergoes a process known as Kasner inversions. Eventually, spacetime terminates at a spacelike Kasner singularity, and it can be proven that there is no Cauchy horizon [106–110].

The rest of the paper is organized as follows. In Sec. II, we begin by constructing the necessary doubly holographic model, ensuring that the geometry of the tensionless brane and all matter fields satisfy the Neumann boundary conditions (NBCs). In Sec. III, we review the holographic superconductors with backreaction. In Sec. IV, we review the internal structure of the black hole in the holographic superconductivity model. In Sec. V, we study the Page curve under bath deformation by calculating the area of the HM surface and the island surface. In the final Sec. VI, we present the conclusions drawn from our study and the work we are interested in for the future.

II. THE DOUBLY HOLOGRAPHIC SETUP

The entire action of the $(d+1)$-dimensional asymptotic AdS_{d+1} spacetime considering a doubly holographic setup reads

$$I = \frac{1}{16\pi G_N^{d+1}}\left[\int_M d^{d+1}x\sqrt{-g}(R-2\Lambda) + 2\int_B d^dx\sqrt{-h}(K-T) + 2\int_\partial d^dx\sqrt{-h_\partial}K_\partial + 2\int_{B\cap\partial} d^{d-1}x\sqrt{-\Sigma}\theta\right] + \int_M d^{d+1}x\sqrt{-g}\mathcal{L}_m. \tag{3}$$

Here, B is the RS brane with tension T, which serves as a gravitational part of the boundary of the bulk spacetime. K is the trace of the extrinsic curvature K_{ab} defined by $K_{ab} = h_a^c \nabla_c n_b$, where n represents the unit normal vector on the brane. The first term in the second line of the above action is the Gibbons-Hawking boundary term, where K_∂ is the trace of the extrinsic curvature on the conformal boundary ∂ (as the nongravitational bath). The second term in the second line of the above action represents the junction term at the intersection of the brane B and conformal boundary ∂. θ is the supplementary angle

[3]To give a different perspective, this is similar to considering CFT matter with a smaller central charge in a double holography model, where one expects corrections to the large-N limit of the AdS/CFT correspondence.

between the brane B and conformal boundary with $\cos(\theta) = n_B \cdot n_\partial$, where n_B and n_∂ are two outward point unit normal vectors at the brane B and conformal boundary ∂. g, h, h_∂, and Σ denote the matrix determinant of M, B, ∂, and $B \cap \partial$, respectively. In this paper, the Lagrangian density $\mathcal{L}_m$ for a Maxwell field and a charged complex scalar field will be considered [65–67]

$$\mathcal{L}_m = -\frac{1}{4}F^2 - |D\phi|^2 - m^2|\phi|^2, \tag{4}$$

where $F = dA$ is the field strength of the gauge field A with $A_t(z) = \mu - \rho z^{d-2}$. Here μ is the chemical potential and ρ a charge density. ϕ is a complex scalar field with mass m. The covariant derivative is defined by $D = \nabla - iqA$, where q is the charge of the charged scalar field. It is important to emphasize that, in order to align with the original theoretical model of holographic superconductors [65–67], we have not considered the topological terms of the gauge field in the brane action and the external magnetic field in the ansatz of the gauge field. In fact, as of now, we still lack a complete description of holographic superconductors within the AdS/BCFT correspondence or the doubly holographic setup, which is an interesting direction for research and we intend to leave it for future completion. This paper could perhaps be understood as an attempt to extend the holographic superconductor model for the first time under the doubly holographic framework.

In the study of quantum Hall systems using the AdS/BCFT, Fujita, Melnikov *et al.* found that for the simple plane-symmetric black hole ansatz, only tensionless RS branes are allowed [111,112]. Moreover, within that context, the influence of the gauge field's topological terms and the external magnetic field proves to be essential. In the research on the AdS/BCFT correspondence and Horndeski gravity, Santos *et al.* also discovered that the plane-symmetric charged 4-dimensional AdS black hole only allows for tensionless RS branes in the $AdS_4/BCFT_3$ construction [113–115]. From the NBC of the gauge field and considering a system with a finite charged density ρ, Jeong *et al.* also found that the tension of the brane should vanish [40] (as seen in the Appendix for the detailed mathematical steps.). Thus, in our paper, for simplicity, we also consider the holographic superconductor with the tensionless brane in doubly holographic model.

When we impose the following NBC on the gravitational part of the boundary, the RS brane is called the Planck brane

$$K_{ab} - (K - T)h_{ab} = 0. \tag{5}$$

We will start with the generic asymptotically AdS_{d+1} planar black hole written in Poincaré coordinates

$$ds^2 = \frac{L^2}{z^2}\left[-f(z)e^{-\chi(z)}dt^2 + \frac{dz^2}{f(z)} + dx_1^2 + \sum_{i=2}^{d-1} dx_i^2\right]. \tag{6}$$

Now, we will consider the surface $z = x_1 \tan\theta$ as the Planck brane, where θ is the supplementary angle between the brane and the conformal boundary, as see in Fig. 2. After computing the extrinsic curvature of the surface

$$K_{ab} = -\frac{\cos\theta}{L}h_{ab}, \tag{7}$$

we can get the tension by using the NBC (5)

$$T = -\frac{(d-1)\cos\theta}{L}. \tag{8}$$

When the tension satisfies the following bound, the RS brane is subcritical tension brane, also known as the Karch-Randall (KR) brane

$$|T| < d - 1. \tag{9}$$

With no scalar field and U(1) gauge field, the induced geometry of the KR brane is pure AdS_d spacetime. However, in this paper, we will consider the bath deformation of a charged scalar field. As a result, the brane is no longer a vacuum solution but a hair black hole. Nevertheless, as long as we find the boundary that satisfy NBC (5), the nonvacuum solution can still be a KR brane. For simplicity in our calculations, we only consider the case where the tension is absent

$$T = 0\left(i.e., \theta = \frac{\pi}{2}\right). \tag{10}$$

In this setup, the brane has no backreaction on the background, but what we concern is the backreaction of the matter field. Due to $\theta = \pi/2$ corresponding to the tensionless limit, for convenience, we can take the hypersurface

$$x_1 = 0, \tag{11}$$

as the position of the brane, as shown in Fig. 2. We must ensure that this hypersurface is indeed the appropriate KR brane, meaning that the background geometry, the charged

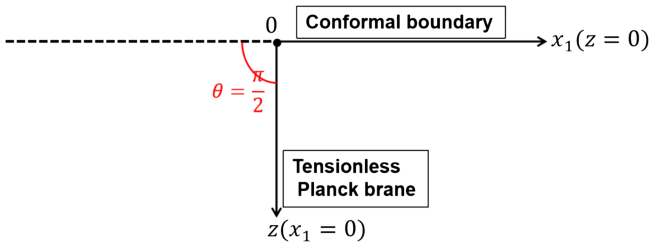

FIG. 2. A schematic diagram of the tensionless Planck brane for the tension $T = 0$ with $\theta = \pi/2$.

scalar field, and the gauge field all satisfy NBC (5), (13), and (14) on the hypersurface. The outward pointing unit normal vector on the hypersurface is $n_\mu = \frac{\delta_{\mu 1}}{z}$, where $\delta_{\mu 1}$ is the Kronecker delta and 1 denotes the x^1 coordinate. then the extrinsic curvature is

$$K_{ab} = h_a^c \nabla_c n_b = 0. \tag{12}$$

We can also find $K_{ab} = 0$ from the result (7) when $\theta = \pi/2$. So this is indeed a tensionless KR brane. For the U(1) gauge field A_μ, we can impose the following NBC without the topological terms on the brane [21,116,117]:

$$F_{\mu\nu} n^\mu h_a^\nu = 0, \tag{13}$$

where h_a^ν is the projection operator which gives the gauge field and induced metric on the brane B: $\bar{A}_a = h_a^\mu A_\mu$ and $h_{ab} = h_a^\mu h_b^\nu g_{\mu\nu}$. As for the charged scalar field [$\phi = \phi(z)$] being independent of the coordinate x_1, it evidently satisfies a NBC [29,118]:

$$n^\mu D_\mu \phi(z) = z D_1 \phi(z) = 0. \tag{14}$$

III. HOLOGRAPHIC SUPERCONDUCTOR MODEL

In this section, we provide a brief overview of the holographic superconductors with the backreaction. For a more in-depth understanding, readers are encouraged to refer to the Refs. [65–67,119–123]. The action of the bulk is the $(d+1)$-dimensional AdS_{d+1} Einstein-Maxwell theory with a scalar field coupling U(1) gauge field

$$I_{\text{bulk}} = \frac{1}{16\pi G_N^{(d+1)}} \int_M d^{d+1}x\sqrt{-g}(R - 2\Lambda) + \int_M d^{d+1}x\sqrt{-g}\left[-\frac{1}{4}F^2 - |D\phi|^2 - m^2|\phi|^2\right], \tag{15}$$

where $G_N^{(d+1)}$ is the $(d+1)$-dimensional Newtonian gravitational constant and we will take $16\pi G_N^{(d+1)} = 1$. R is the Ricci scalar of spacetime. The negative cosmological constant is

$$\Lambda = -\frac{d(d-1)}{2L^2}, \tag{16}$$

where L is the AdS radius and we will set $L = 1$ from here. We will consider the following ansatz for the generic asymptotically AdS_{d+1} planar black hole and matter fields:

$$ds^2 = \frac{1}{z^2}\left[-f(z)e^{-\chi(z)}dt^2 + \frac{dz^2}{f(z)} + \sum_{i=1}^{d-1} dx_i^2\right], \tag{17}$$

$$\phi = \phi(z), \qquad A_\mu dx^\mu = A_t(z)dt. \tag{18}$$

The Hawking temperature is

$$T_H = -\left.\frac{f'(z)e^{-\chi(z)/2}}{4\pi}\right|_{z=z_h}. \tag{19}$$

We can get the equations of motion with four functions: $\phi(z)$, $A_t(z)$, $\chi(z)$, $f(z)$

$$\phi'' - \left(\frac{d-1}{z} - \frac{f'}{f} + \frac{\chi'}{2}\right)\phi' + \left(\frac{q^2 A_t^2 e^\chi}{f^2} - \frac{m^2}{z^2 f}\right)\phi = 0, \tag{20}$$

$$A_t'' - \left(\frac{d-3}{z} - \frac{\chi'}{2}\right)A_t' - \frac{2q^2 A_t \phi^2}{z^2 f} = 0, \tag{21}$$

$$\chi' - \frac{2}{d-1}\left(z\phi'^2 + \frac{zq^2 A_t^2 \phi^2}{f^2}e^\chi\right) = 0, \tag{22}$$

$$f' + \frac{d}{z} - \left(\frac{d}{z} + \frac{\chi'}{2}\right)f - \frac{1}{d-1}\left(\frac{z^3 A_t'^2 e^\chi}{2} + \frac{m^2\phi^2}{z}\right) = 0, \tag{23}$$

where the prime denotes the derivative with respect to z. For $\phi = 0$, the analytical solution to the above equations of motion is the familiar $(d+1)$-dimensional AdS_{d+1}-RN black hole

$$f(z) = 1 - \frac{z^d}{z_h^d} - \frac{d-2}{2(d-1)}\left(\frac{z^d}{z_h^d} - \frac{z^{2d-2}}{z_h^{2d-2}}\right)z_h^{2d-2}\rho^2, \quad \rho = \frac{\mu}{z_h^{d-2}}, \tag{24}$$

$$A_t(z) = \mu\left(1 - \frac{z^{d-2}}{z_h^{d-2}}\right), \qquad \chi(z) = 0, \tag{25}$$

where z_h is the event horizon with $f(z_h) = 0$, μ is the chemical potential, and ρ is the charge density. The Hawking temperature for AdS_{d+1}-RN black hole is

$$T_{\text{RN}} = \frac{1}{z_h}\left[\frac{d}{4\pi} - \frac{(d-2)^2 z_h^{2d-2}\rho^2}{8\pi(d-1)}\right]. \tag{26}$$

For $\phi \neq 0$, we can expand the equations of motion (20)–(23) near the horizon ($z \to z_h$) as considering $f(z_h) = 0$, $A_t(z_h) = 0$:

$$\phi(z) = \phi_0 + \phi_1(z - z_h) + \phi_2(z - z_h)^2 + \cdots, \tag{27}$$

$$A_t(z) = A_1(z - z_h) + A_2(z - z_h)^2 + \cdots, \tag{28}$$

$$\chi(z) = \chi_0 + \chi_1(z - z_h) + \chi_2(z - z_h)^2 + \cdots, \tag{29}$$

$$f(z) = f_1(z - z_h) + f_2(z - z_h)^2 + \cdots. \tag{30}$$

Using the numerical shooting method, we can determine three constants ϕ_0, A_1, and χ_0 that yield solutions satisfying

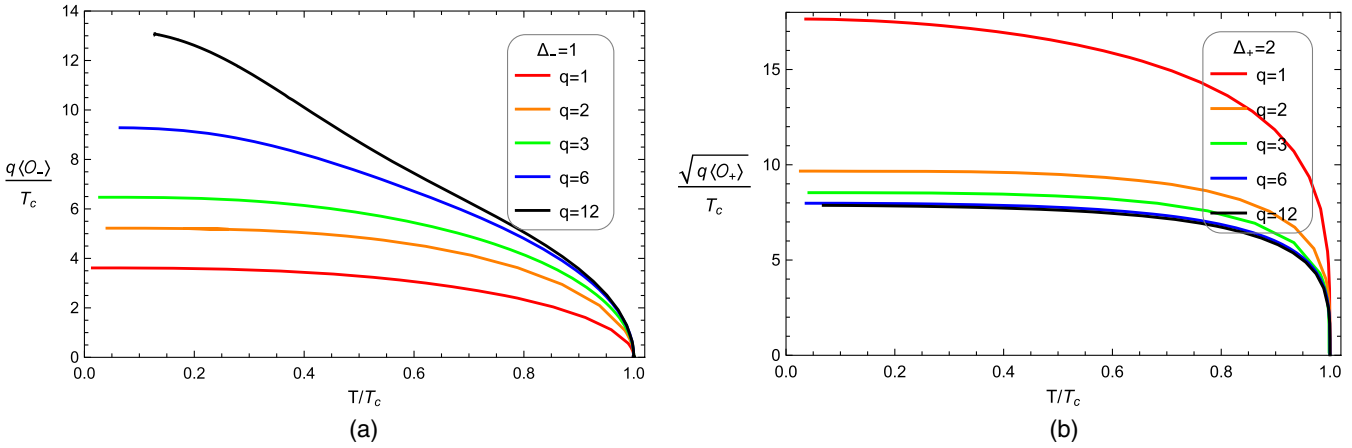

FIG. 3. The value of the condensate as a function of the temperature, with the fixed charge of the scalar field, for two operators $\mathcal{O}_-$ and $\mathcal{O}_+$ with conformal dimensions Δ_- and Δ_+, respectively.

the above equations of motion (20)–(23) and the following boundary conditions: Near the boundary $z \to 0$, the equations of motion (20)–(23) have asymptotic solutions:

$$\phi(z) \approx \phi_- z^{\Delta_-} + \phi_+ z^{\Delta_+}, \qquad A_t(z) \approx \mu - \rho z^{d-2},$$
$$\chi(z) \approx 0, \qquad f(z) \approx 1, \tag{31}$$

where the conformal dimension $\Delta_\pm$ is the dimension of the operator

$$\Delta_\pm = \frac{d}{2} \pm \sqrt{\frac{d^2}{4} + m^2}. \tag{32}$$

We can easily note that $\Delta = \Delta_\pm$ satisfy a mass-dimension renormalization

$$\Delta(\Delta - d) = m^2. \tag{33}$$

The AdS boundary is vacuum-stable only if $m^2 \geq m_{\mathrm{BF}}^2$. $m_{\mathrm{BF}}^2 = -d^2/4$ is the Breitenlohner-Freedman (BF) bound. When $m^2 = m_{\mathrm{BF}}^2$, we have $\Delta_- = \Delta_+ = d/2$. For $-d^2/4 \leq m^2 < -d^2/4 + 1$, there are two quantization schemes: according to the AdS/CFT dictionary, ϕ_+ is the vacuum expectation value $\langle \mathcal{O}_+ \rangle$, while ϕ_- is regarded as the source of the dual operator $\mathcal{O}$ and should vanish ($\phi_- = 0$), or ϕ_- is the vacuum expectation value $\langle \mathcal{O}_- \rangle$, while ϕ_+ is regarded as the source of the dual operator $\mathcal{O}$ and should vanish ($\phi_+ = 0$). For $m^2 \geq -d^2/4 + 1$, only the Δ_+-mode can be normalized. In Fig. 3, we provide the condensation of these two operators with different charges. Note that we have fixed the dimension and the mass of the scalar field (i.e., $d = 3$, $m^2 = -2$). Unless otherwise stated, we maintain this setup in the following calculations.

IV. KASNER SOLUTIONS OF HOLOGRAPHIC SUPERCONDUCTORS

As mentioned in the introduction, the interior of the black hole with charged scalar hair exhibits intricate dynamical behaviors. For instance, the relevant deformations can lead to the disappearance of the Cauchy horizon, triggering several distinct dynamical regimes within the black hole interior. These are the collapse of the ER bridge, Josephson oscillations, Kasner universe, and in some cases, a final Kasner inversion before reaching the Kasner singularity. We will not delve into a detailed exposition of the complete picture. Instead, we will provide a concise overview of the Kasner solutions. Readers interested in a more in-depth understanding of the details are encouraged to refer to Refs. [104–110,124].

Near the singularity ($z \to \infty$), we assume that we can neglect the A_t' term in Eq. (23), the scalar-mass term, and its charged term. Then these equations of motion (20)–(23) approximate into

$$\phi'' - \left(\frac{d-1}{z} - \frac{f'}{f} + \frac{\chi'}{2}\right)\phi' = 0, \tag{34}$$

$$A_t'' - \left(\frac{d-3}{z} - \frac{\chi'}{2}\right)A_t' = 0, \tag{35}$$

$$\chi' - \frac{2z\phi'^2}{d-1} = 0, \tag{36}$$

$$f' - \left(\frac{d}{z} + \frac{\chi'}{2}\right)f = 0. \tag{37}$$

The solutions of these equations are

$$\phi = \alpha\sqrt{d-1}\log z, \qquad A_t' = A_o z^{-3+d-\alpha^2},$$
$$\chi = 2\alpha^2 \log z + \chi_o, \qquad f = -f_o z^{d+\alpha^2}, \tag{38}$$

where α, A_o, and f_o are integration constants. By using the solutions (38), we can get metric components g_{tt} and g_{zz}

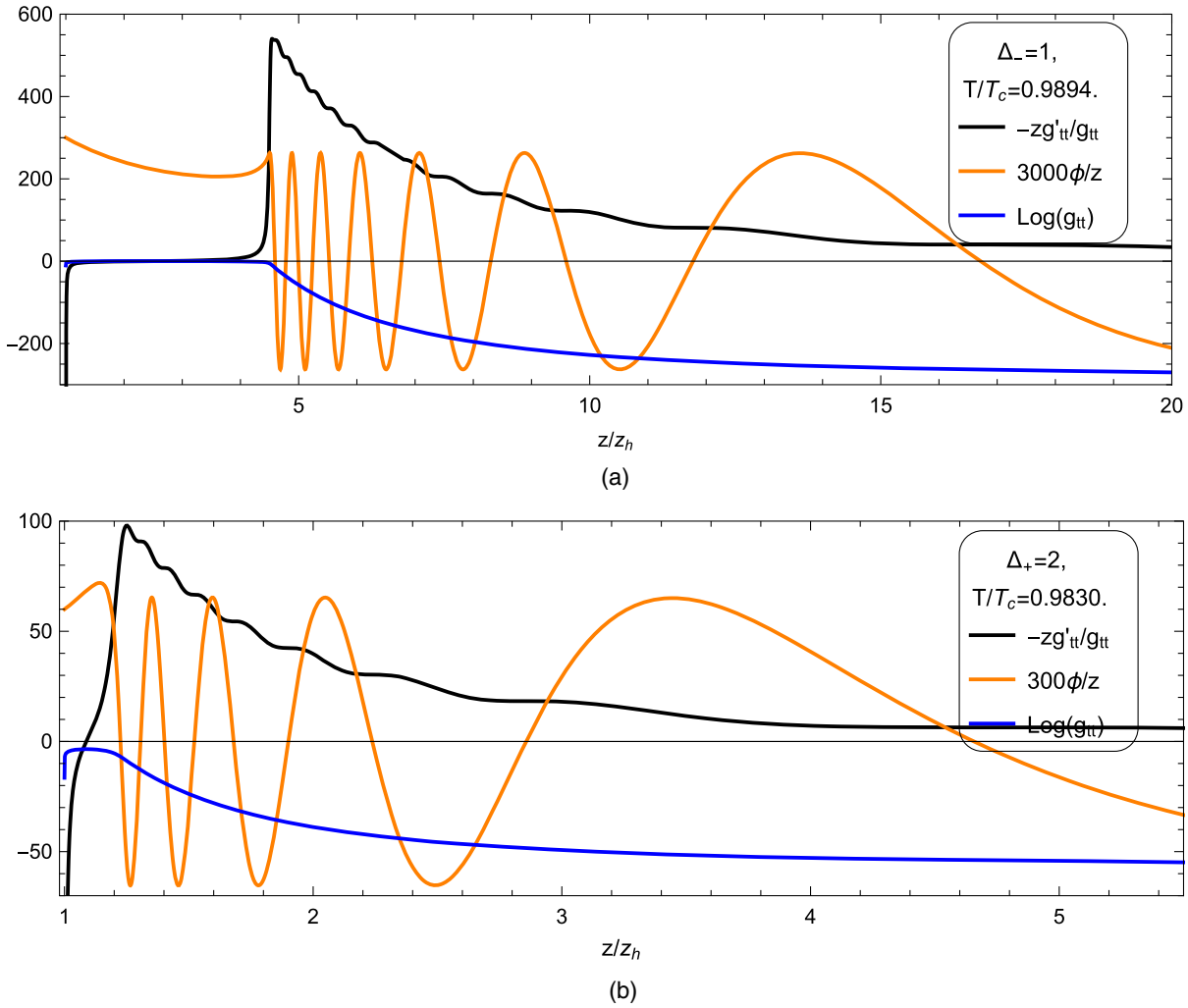

FIG. 4. $-z\frac{g'_{tt}}{g_{tt}}$, $3000\frac{\phi}{z}$, $300\frac{\phi}{z}$, $\log(g_{tt})$ are plotted as a function of the radial coordinate z/z_h for the two conformal dimensions and corresponding temperatures (a) $\Delta_- = 1$, $T/T_c = 0.9894$; (b) $\Delta_+ = 2$, $T/T_c = 0.9830$.

$$g_{tt} = -\frac{fe^{-\chi}}{z^2} = f_o e^{-\chi_o} z^{-2+d-\alpha^2},$$
$$g_{zz} = \frac{1}{z^2 f(z)} = -\frac{z^{-2-d-\alpha^2}}{f_o}. \tag{39}$$

We have plotted $-zg'_{tt}/g_{tt}$, ϕ/z, $\log(g_{tt})$ as a function of z/z_h for two different conformal dimensions $\Delta_\pm$ in Fig. 4. We can find the distinct epochs of the collapse of the ER bridge and Josephson oscillations from the figure. The metric also captures the behaviors of the oscillations. Consider the following parameter transformations

$$\tau = c_\tau z^{-\frac{d+\alpha^2}{2}}, \qquad \left(c_\tau = \frac{2}{(d+\alpha^2)\sqrt{f_o}}\right), \tag{40}$$

we can obtain the following Kasner solutions near the singularity of the spacetime [125–127]:

$$ds^2 = -d\tau^2 + c_t \tau^{2p_t} dt^2 + c_x \tau^{2p_x} d\vec{x}^2_{d-1}, \quad \phi \sim -p_\phi \log\tau, \tag{41}$$

$$c_t = \frac{f_o e^{-\chi_o}}{c_\tau^{2p_t}}, \qquad c_x = \frac{1}{c_\tau^{2p_x}}, \tag{42}$$

where the Kasner exponents $\{p_t, p_x, p_\phi\}$ are

$$p_t = \frac{2-d+\alpha^2}{d+\alpha^2}, \quad p_x = \frac{2}{d+\alpha^2}, \quad p_\phi = \frac{2\sqrt{d-1}\alpha}{d+\alpha^2}, \tag{43}$$

which satisfy the Kasner constraints

$$p_t + (d-1)p_x = 1, \quad p_t^2 + (d-1)p_x^2 + p_\phi^2 = 1. \tag{44}$$

When $p_t < 0$, corresponding to an ER bridge grows, describe a "Kasner inversion" $\alpha \to 1/\alpha$ in which

$$p_t \to -\frac{p_t}{2p_t+1}. \tag{45}$$

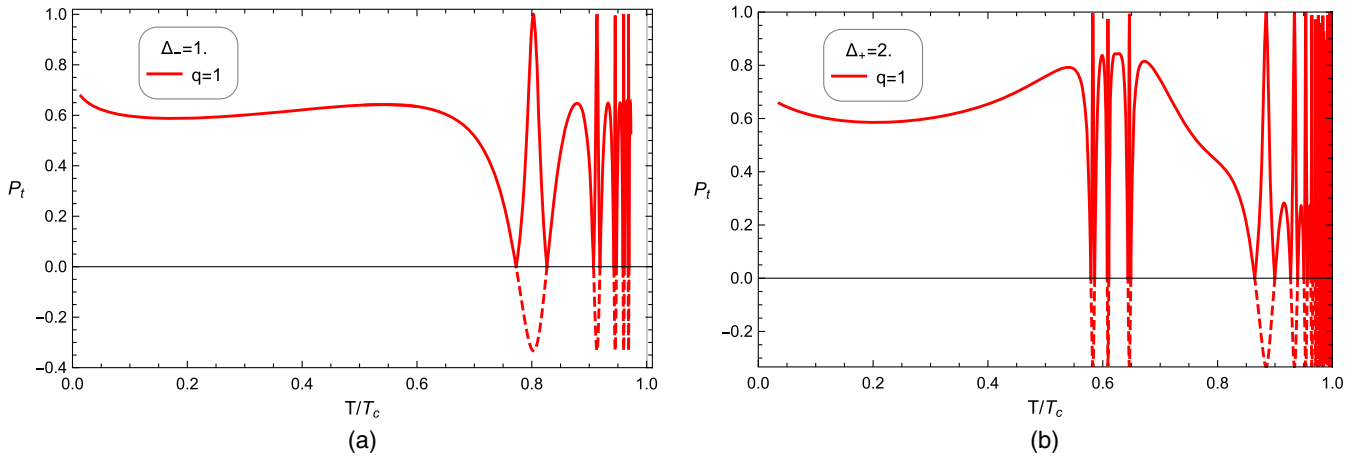

FIG. 5. The Kasner exponent p_t as a function of the temperature T/T_c after inversions. We have also shown $p_t < 0$ before inversions as a dashed red line.

In this case, the Kasner exponent p_t changes its sign in the inversions at late times. The first discovery of this inversion was made by Hartnoll and his collaborators in [104,105]. In Fig. 5, we show the variations of p_t with T/T_c for two different conformal dimensions $\Delta_\pm$ as charge ($q = 1$). The strong oscillations are shown near the critical temperature T_c. These oscillations in the Kasner exponents also reflect the imprint of Josephson oscillations.

V. BATH DEFORMATIONS AND PAGE CURVES

This section constitutes the central component of our article. Building upon the inspiration from the paper [29], we investigate the Page curves for the eternal AdS_{d+1} charged black hole within the context of a doubly holographic model, where the BCFT's states in the conformal bath are deformed by a charged scalar field. The specific setup of this model is as follows: initially, we couple the brane with the conformal bath and impose a transport boundary condition at the interface between the brane and the conformal bath, bringing them to thermodynamic equilibrium. As the Hawking radiation reaches the Page time, an interior region called the "island" forms within the black hole (sometime, the island is outside the horizon [3]), causing the computed entanglement entropy of the radiation region to no longer increase continuously but instead exhibit an initial rise followed by a plateau. The resulting Page curves for this setup are termed the version of the eternal black hole, as shown in Fig. 1(c).

A. Growth area of the Hartman-Maldacena surfaces

Before Page time, there is no contribution from the island region. The candidate extremal surface is the time-dependent HM surface [47]. As time progresses, the extremal surface gets progressively closer to a specific critical radius within the interior of the black hole. At late times, the area of the extremal surface increases linearly with time. When it gets close to the critical radius, the growth velocity of the extremal surface tends toward a constant value, which we call the entanglement velocity [47,102,128]. Since the entanglement velocity is highly sensitive to the geometric properties of the black hole's interior but not to the near-singularity region, we can use it as a probe for exploring the interior of the black hole. We will briefly explain this fact and apply it to our model. Following the method applied in [21,29,129], we will investigate the time evolution of the HM surface in doubly holographic framework. First, considering a constant-$x_1 = x_{\mathcal{R}}$ slice, the induced metric takes the following form:

$$ds^2|_{x_1=x_{\mathcal{R}}} = \frac{1}{z^2}\left[-f(z)e^{-\chi(z)}dt^2 + \frac{dz^2}{f(z)} + \sum_{i=2}^{d-1} dx_i^2\right]. \quad (46)$$

For a time-dependent surface $[z = z(t)]$, the area function is

$$A = V_{d-2}\int \frac{dt}{z(t)^{d-1}}\sqrt{-f[z(t)]e^{-\chi[z(t)]} + \frac{\dot{z}(t)^2}{f[z(t)]}}, \quad \dot{z} = \frac{dz}{dt}, \quad (47)$$

where $V_{d-2} = \int \prod_{i=2}^{d-1} dx_i$ is an overall volume factor. Since the volume factor is a constant, for convenience, we can define the HM area density (which we will also refer to as "area") and its corresponding Lagrangian

$$\mathcal{A}_{\mathrm{HM}} = \frac{A}{V_{d-2}} = \int \frac{dt}{z(t)^{d-1}}\sqrt{-f[z(t)]e^{-\chi[z(t)]} + \frac{\dot{z}(t)^2}{f[z(t)]}} = \int dt\mathcal{L}. \quad (48)$$

Due to the explicit time-independent Lagrangian, we can identify that the "energy" E of the minimal surface is a

constant of motion

$$E = \dot{z}\frac{\partial \mathcal{L}}{\partial \dot{z}} - \mathcal{L} = \frac{f(z)e^{-\chi(z)}}{z^{d-1}\sqrt{-f(z)e^{-\chi(z)} + \frac{\dot{z}^2}{f(z)}}}, \tag{49}$$

and the minimal surface has the following expression:

$$\dot{z} = \pm f(z)e^{-\chi(z)/2}\sqrt{1 + \frac{f(z)e^{-\chi(z)}}{z^{2(d-1)}E^2}}. \tag{50}$$

If there exists a location inside a black hole with a radius of z_* satisfying the condition ($\frac{dz}{dt}|_{z=z_*} = 0$), we can readily derive the constant E

$$E^2 = -\frac{f(z_*)e^{-\chi(z_*)}}{z_*^{2(d-1)}}. \tag{51}$$

By substituting (50) into (48), and taking $dt = \frac{dz}{\dot{z}}$ into account, we can get the area expression of the HM surface[4]

$$\mathcal{A}_{\mathrm{HM}}(t_b) = 2\int_0^{z_*} \frac{dz}{z^{d-1}\sqrt{f(z) + e^{\chi(z)}z^{2(d-1)}E^2}}. \tag{52}$$

Considering the following integral:

$$\int_0^{z_*} \frac{dz}{\dot{z}} = \int_{t_b}^{t_*} dt = t_* - t_b, \tag{53}$$

and the symmetry geodesic argument at the turning point ($t_*(z = z_*) = 0$), we can get the boundary time

$$t_b = -P\int_0^{z_*} \frac{\mathrm{sgn}(E)e^{\chi/2}dz}{f(z)\sqrt{1 + f(z)e^{-\chi(z)}/z^{2(d-1)}E^2}}, \tag{54}$$

where P and $\mathrm{sgn}(E)$ denote the principal value and the sign of the "energy" E, respectively. Using the area expression (52) and boundary time (54), we can numerically compute the time-dependent area of the HM surface. To get the late-time behavior ($t_b \to \infty$), let us first consider the following function

$$g(z) = -\frac{f(z)e^{-\chi(z)}}{z^{2(d-1)}}. \tag{55}$$

After substituting the Kasner solutions (38) into function $g(z)$ (55), we can find

$$g(z_h) = 0, \qquad \lim_{z\to\infty} g(z) = \lim_{z\to\infty} f_0 e^{-\chi_0} z^{2-d-\alpha^2} = 0,$$
$$g(z)|_{z>z_h} > 0. \tag{56}$$

So, there is a critical radius z_c inside the black hole that maximizes $g(z)$, and the critical radius also satisfies (51)

$$E_c^2 + \frac{f(z_c)e^{-\chi(z_c)}}{z_c^{2(d-1)}} = 0. \tag{57}$$

When $z_* \to z_c$, the boundary time diverges ($t_b \to \infty$). Next, by performing the derivative for the area expression of HM surface $\mathcal{A}_{\mathrm{HM}}$ (52) with boundary time t_b (54) while also taking $f(z_c) < 0$ into account, we can readily obtain the growth rate of the HM surface area with respect to the boundary time

$$\frac{\partial \mathcal{A}_{\mathrm{HM}}}{\partial t_b} = 2\frac{-f(z_c)e^{-\chi(z_c)}}{z_c^{2(d-1)}|E_c|} = 2\sqrt{-\frac{f(z_c)e^{-\chi(z_c)}}{z_c^{2(d-1)}}} = \frac{2v}{z_h^{d-1}}, \tag{58}$$

where v is the entanglement velocity. For the AdS_{d+1}-Schwarzschild brane, the entanglement velocity is

$$v_{\mathrm{AS}} = \frac{\sqrt{d}(d-2)^{\frac{d-2}{2d}}}{[2(d-1)]^{\frac{d-1}{d}}}. \tag{59}$$

For the AdS_{d+1}-RN brane, the entanglement velocity is

$$v_{\mathrm{ARN}} = \sqrt{\frac{d - 2^{3-\frac{4}{d}}z_h^{2d-2}\rho^2(d-1)^{3-\frac{4}{d}}(d-2)^{\frac{2}{d}}[2(d-1) + (d-2)z_h^{2d-2}\rho^2]^{\frac{2}{d}-2}}{2^{4-\frac{4}{d}}(d-1)^{4-\frac{4}{d}}(d-2)^{\frac{2}{d}-1}[2(d-1) + (d-2)z_h^{2d-2}\rho^2]^{\frac{2}{d}-2}}}. \tag{60}$$

In Fig. 6, we show the entanglement velocity v as a function of the Kasner exponent p_t before the inversions. We find that the entanglement velocity can not only probe the interior of the black hole but also probe the Josephson oscillations, which is significantly different from the solutions that deformed by a neutral scalar field [29,102,103,130]. In Fig. 7, we show the entanglement velocity v as a function of the bath deformation $q\phi_\pm$ and the temperature T/T_c. When the deformation turn off ($q\phi_\pm = 0$), by comparing the critical entanglement velocity in Figs. 7(a) and 7(b) with the same charge, we find that the critical entanglement velocity will change with the conformal dimension. This behavior is different from the neutral case [29], wherein the critical entanglement velocity does not change with the conformal dimension. This is not surprising at all. When there is no backreaction, our geometry is an

[4]The factor of 2 in front of the integral is due to the consideration of two side black hole.

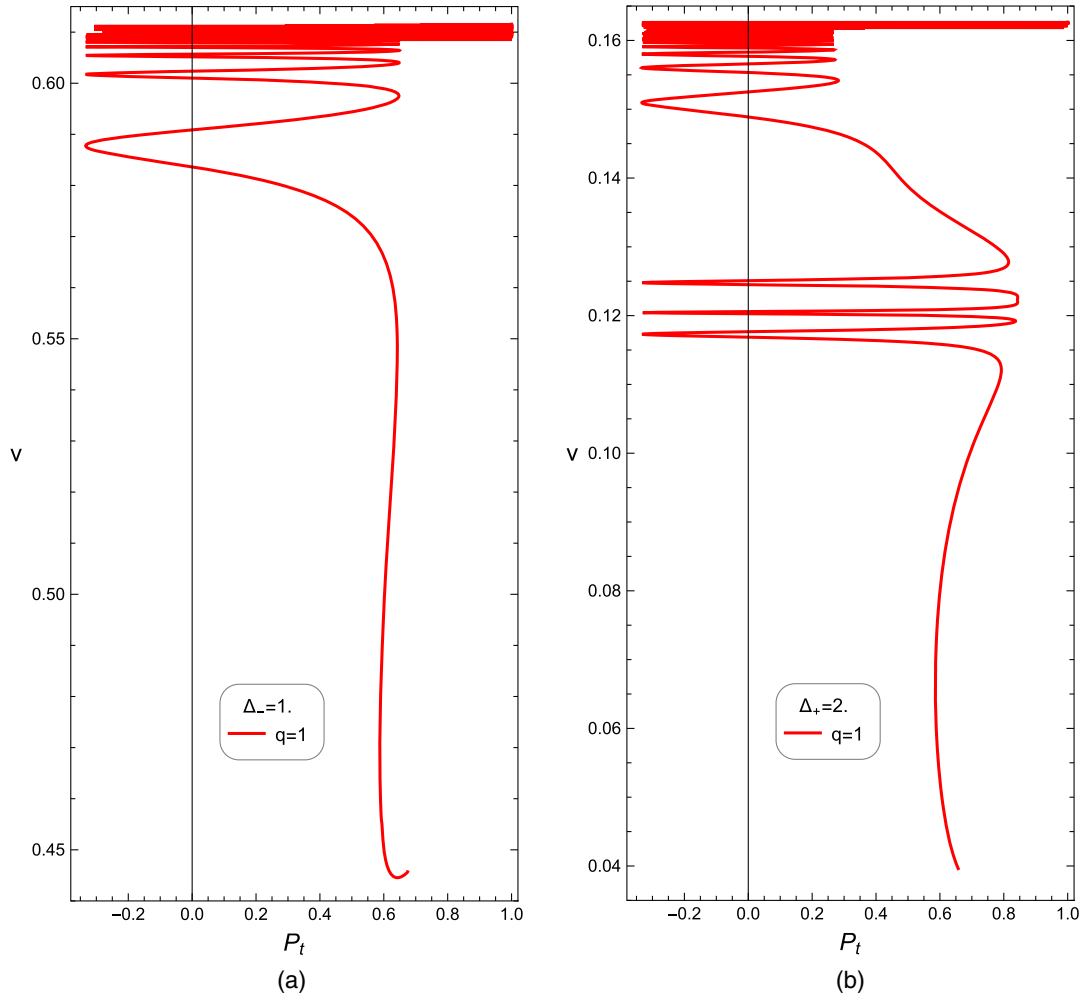

FIG. 6. The entanglement velocity v as a function of the Kasner exponent p_t for the charge ($q = 1$) before the Kasner inversions.

AdS-RN black hole. The critical temperature will change with different conformal dimensions, and fundamentally depends on the charge density ρ of the black hole. In the case of neutral deformation, without backreaction, the geometry is just an AdS-Schwarzschild black hole, and its temperature is independent of the conformal dimension. Similarly, the critical Page point, critical initial area difference, and critical Page time that we will discuss later all change with varying conformal dimensions.

Furthermore, we also observe that the behaviors of the entanglement velocity are related to the charges. When the charge is small (e.g., when $q = 1$), the entanglement velocity initially decreases with an increase in deformation (or a decrease in temperature), then slightly increases again as it approaches zero temperature. It is worth noting that this behavior is more pronounced in the case of $\Delta_- = 1$. When the charge is large (e.g., when $q = 12$), the entanglement velocity increases initially with deformation, then decreases. This behavior is more pronounced for $\Delta_+ = 2$ [as seen Figs. 7(b) and 7(f) for the curves of $q = 2, 3, 6$, and 12]. It is important to emphasize that the entanglement velocity will significantly impact on the Page time that we will investigate later. In specific, an increase in the entanglement velocity with the deformation will lead to a decrease in the Page time, even the temperature decreases.

From subfigures (d), (e), (g), and (h) of Fig. 7, we can observe that at the critical temperature T_c, the slope of the entanglement velocity shows a clear discontinuity between the superconducting ($T < T_c$) and normal phases ($T > T_c$), which indicates that the entanglement velocity can serve as a probe for superconducting phase transitions. Furthermore, when we focus our attention on the difference in the entanglement velocity between the superconducting phase and the normal phase at the same temperature, we find a smaller entanglement velocity difference for the charge ($q = 12$) compared to the charge ($q = 1$), which is clear because the larger charge, the closer it approaches the probe limit ($q \to \infty$).

B. Area of the island surface

As we mentioned in the introduction, to obtain the Page curves, the initial area of the HM surface must be smaller

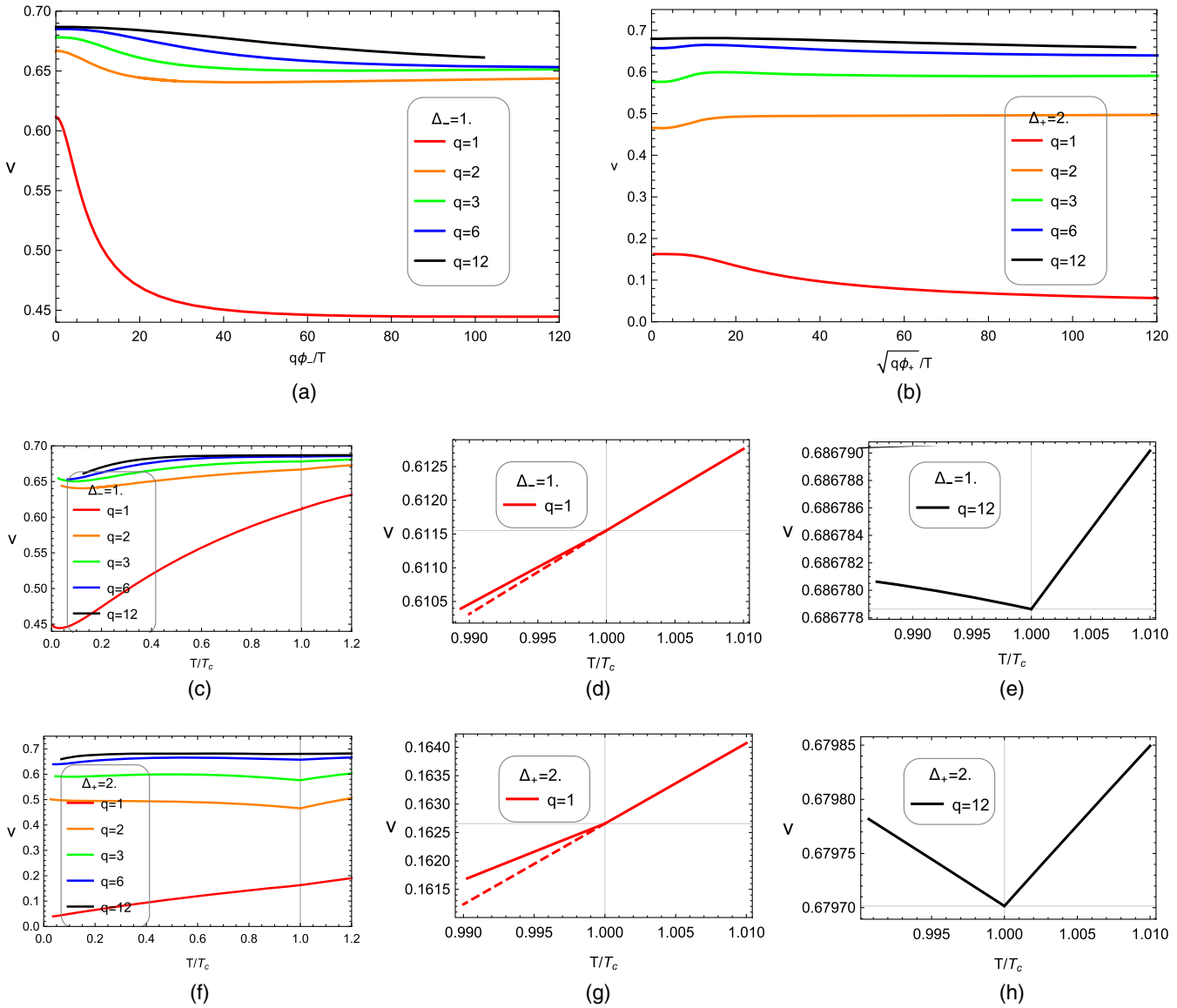

FIG. 7. The entanglement velocity v as a function of the deformation (a) $q\phi_-/T$; (b) $\sqrt{q\phi_+}/T$ for different charges. (c),(f) represent the variation of the entanglement velocity v with the temperature T/T_c, while (d),(e),(g),(h) represent the situation near the critical temperature for the charge ($q = 1$) and ($q = 12$). To visually observe the transition of the entanglement velocity's slope at the critical temperature, in the (d),(g), we use a dashed line to represent the entanglement velocity corresponding to the normal phase extending below the critical temperature.

than the area of the island surface. This imposes a particular constraint on values of $x_{\mathcal{R}}$ regardless of the temperature and conformal dimension. Specifically, the value of $x_{\mathcal{R}}$ must be larger than a critical point (the Page point) [17,21,29]. We start from the induced metric for the time slice ($t = 0$)

$$ds^2|_{t=0} = \frac{1}{z^2}\left(\frac{dz^2}{f} + dx_1^2 + \sum_{i=1}^{d-2} dx_i^2\right). \tag{61}$$

Parameterize the coordinate x_1 as a function of z, such that for any surface $[x(z) = x_1(z)]$, the area function takes the following form

$$A = V_{d-2}\int \frac{dz}{z^{d-1}}\sqrt{\frac{1}{f(z)} + \dot{x}(z)^2}, \qquad \dot{x} = \frac{dx_1}{dz}, \tag{62}$$

where $V_{d-2} = \int dx_2 \cdots dx_{d-1}$ is an overall volume factor. Following the steps for calculating the area of the HM surfaces in the previous section, we define the area density $\mathcal{A}_I$ and its Lagrangian $\mathcal{L}$ for the island surface

$$\mathcal{A}_I = \frac{A}{V_{d-2}} = \int \frac{dz}{z^{d-1}}\sqrt{\frac{1}{f(z)} + \dot{x}(z)^2} = \int dz\mathcal{L}. \tag{63}$$

Then, we should minimize the area density $\mathcal{A}_I$ and get the extremal surface that satisfies the Euler-Lagrangian equation

$$\frac{\partial \mathcal{L}}{\partial x} - \frac{\partial^2 \mathcal{L}}{\partial z \partial \dot{x}} = 0, \tag{64}$$

which indicates that $\partial\mathcal{L}/\partial\dot{x}$ is a constant of motion

$$\frac{\dot{x}(z)}{z^{d-1}\sqrt{\frac{1}{f(z)} + \dot{x}(z)^2}} = C. \tag{65}$$

The boundary conditions for the extremal surface are

$$x(0) = x_{\mathcal{R}}, \qquad \frac{1}{\dot{x}(z)}\bigg|_{z=z_T} = 0, \tag{66}$$

where z_T is the turnaround point. This point represents the boundary of the island region on the brane. Using the Neumann condition, the constant of motion (65) becomes

$$\frac{\dot{x}(z)}{z^{d-1}\sqrt{\frac{1}{f(z)} + \dot{x}(z)^2}} = \pm\frac{1}{z_T^{d-1}}$$
$$\Rightarrow \dot{x}(z) = \pm\frac{z^{d-1}}{\sqrt{f(z)\left[z_T^{2(d-1)} - z^{2(d-1)}\right]}}. \tag{67}$$

Using the Dirichlet boundary condition, we have

$$x_{\mathcal{R}} = \int_0^{x_{\mathcal{R}}} dx = \int_0^{z_T} dz \frac{z^{d-1}}{\sqrt{f(z)[z_T^{2(d-1)} - z^{2(d-1)}]}}. \tag{68}$$

From the above equation, it is evident that given a value of $x_{\mathcal{R}}$, the turnaround point z_T can be determined. By substituting (67) into (63), we can obtain the area of the island surface for a giving $x_{\mathcal{R}}$

$$\mathcal{A}_I = 2\int_0^{z_T} \frac{dz}{z^{d-1}\sqrt{f(z)}} \frac{z_T^{d-1}}{\sqrt{z_T^{2(d-1)} - z^{2(d-1)}}}. \tag{69}$$

For the initial HM surface ($t_b = 0$), according to Eq. (54), it can be solved that $E = 0$, and then, based on Eq. (51), it is solved that $z_* = z_h$. Lastly, according to expression (52), we can derive the following expression for the initial HM surface

$$\mathcal{A}_{\mathrm{HM}}(t_b = 0) = 2\int_0^{z_h} \frac{dz}{z^{d-1}\sqrt{f(z)}}. \tag{70}$$

As mentioned at the beginning of this section, there is a Page curve if and only if $\mathcal{A}_{\mathrm{HM}}(0) < \mathcal{A}_I$. In other words, the initial area difference should satisfy

$$\Delta\mathcal{A}(0) = \mathcal{A}_I - \mathcal{A}_{\mathrm{HM}}(0) > 0. \tag{71}$$

Since the area of the island surface depends on $x_{\mathcal{R}}$, a critical Page point ($x_p = x_{\mathcal{R}}$) that satisfied $\Delta\mathcal{A}(0) = 0$ should be found. Considering that the island surface is also related to the external structure of a black hole, the initial area difference can be utilized to reflect the external back-reaction. Another important thing to note is that near the boundary ($z \to 0$), both of the areas are divergent due to the empty AdS_{d+1} geometry so we will renormalize them by setting a cutoff ($\epsilon = z/z_h \ll 1$). The dimensionless divergent term is

$$z_h^{d-2}\mathcal{A}_\infty = \frac{2}{(d-2)}\frac{1}{\epsilon^{d-2}}. \tag{72}$$

In Figs. 8(a) and 8(b), we show the finite part of the initial area difference $\Delta\mathcal{A}(0)$ as a function of $x_{\mathcal{R}}/z_h$ at the critical temperature. The calculation at this step is to obtain the Page point, which is the critical value of $x_{\mathcal{R}}$, where the area of the island surface is equal to the area of the initial HM surface. From Fig. 8(c), we find that the Page point decreases as the charge increases at critical temperature, which provides a helpful clue for us to need later to fix $x_{\mathcal{R}}$. In Figs. 8(d) and 8(e), we also investigate the influence of scalar deformations ($q\phi_\pm$) on the Page point. We observe that the Page point decreases as the deformation increases, indicating that black holes require fewer radiation degrees of freedom to produce the Page curve. In other words, in the case of stronger deformations at the conformal boundary, the radiation region $\mathcal{R}$ requires more degrees of freedom to ensure the existence of the Page curve, which provides a helpful clue for us to obtain the Page curve, by fixing a reasonable endpoint $x_{\mathcal{R}}$ of the radiation region $\mathcal{R}$. Specifically, if we choose $x_{\mathcal{R}}$ larger than the critical Page point (i.e., the Page point with zero deformation $q\phi_\pm = 0$), then, subsequently, no matter how much the scalar deformation increases, we can have a Page curve uniquely associated with scalar deformation, which implies that the Page curve for a specific radiation region can probe Kasner flows [29].

C. Entanglement entropy and Page curves

We are now computing the Page curves for various charges and two conformal dimensions. Based on the analysis in the previous section, we learn that to get the Page curve, the value of $x_{\mathcal{R}}$ needs to be larger than the Page point. Since the Page point decreases as the charge and deformation increase, to make sure that we always have the Page curve and a finite Page time regardless of the charge and scalar deformation, we will set $x_{\mathcal{R}}$ to be twice the critical Page point for charge $q = 1$. More specifically, we will fix $x_{\mathcal{R}}$

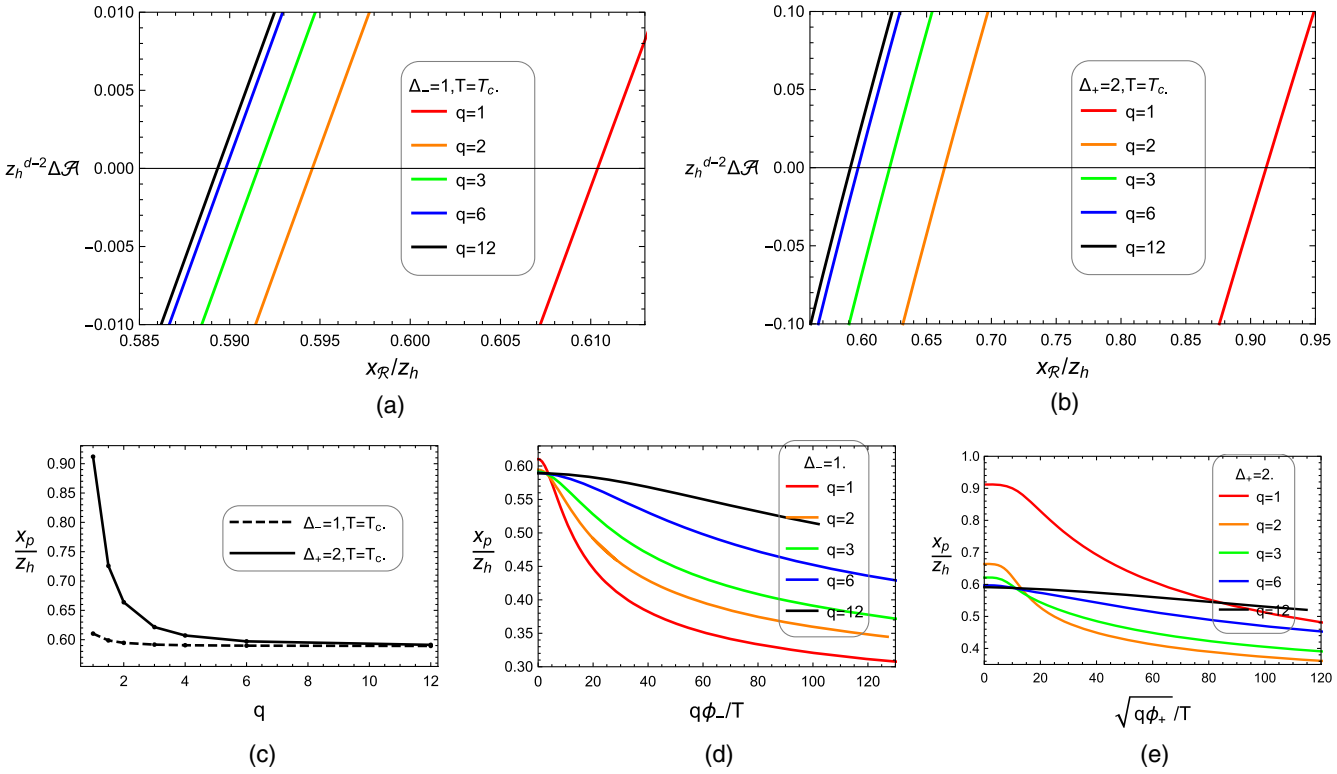

FIG. 8. The area difference $\Delta\mathcal{A}(0)$ versus $x_{\mathcal{R}}$ for different charges with the conformal dimension (a) $\Delta_- = 1$; (b) $\Delta_+ = 2$ at critical temperature $T = T_c$. (c) The Page point x_p as a function of the charge at critical temperature. The Page point x_p as a function of bath deformations (d) $q\phi_-/T$; (e) $\sqrt{q\phi_+}/T$.

$$x_{\mathcal{R}} = 2\frac{x_p}{z_h} = \begin{cases} 2\times 0.610, & (\Delta_- = 1), \\ 2\times 0.912, & (\Delta_+ = 2). \end{cases} \tag{73}$$

To obtain the Page curves, we calculate the entanglement entropy of the radiation region using the time-dependent HM surface that discussed in Sec. V A before Page time. After the Page time, the entanglement entropy of the radiation region is provided by the island surface that discussed in Sec. V B. Since the island surface is time-independent, the entanglement entropy of the radiation region $\mathcal{R}$ no longer continues to increase after the Page time. So, the Hawking radiation satisfies the unitarity of quantum mechanics.

In Fig. 9, we present the Page curves of the systems at the critical temperature [(a), (b)] and semi-critical temperature [(c), (d)] for both conformal dimensions $\Delta_\pm$. From subfigures (a), (b), we can observe that when the system is at the critical temperature, the Page time decreases with the charge growth, which is because as the charge increases, the critical temperature of the boundary system also increases. According to holographic duality, the Hawking radiant temperature of the black hole increases, leading to a faster saturation of the radiant entanglement entropy. However, when considering scalar deformations in the bath, the conventional pattern of higher temperature leading to shorter Page time is not necessarily valid. Specifically, in subfigures (c), (d), we investigate the Page curves where the temperature is reduced to half the critical temperature. Clearly, at this point, the influence of scalar deformations and conformal dimensions becomes significant. By comparing subfigures (a), (c), it may initially appear that as the temperature decreases, the Page time becomes longer. However, when we carefully examine the green curve which corresponding to $\Delta_+ = 2$ and $q = 3$ in subfigures (b), (d), we can observe that despite the temperature reduction, the Page time does not increase; instead, it decreases. In Fig. 11, we can see more intuitively that in some cases, with increasing deformation and decreasing temperature, the Page time does not increase but rather decreases. Furthermore, we also note that the entanglement velocity increases with increasing charge, in accordance with the results in Fig. 7. Finally, it should be noted that the negative values exhibited in the early stage of the Page curve in Fig. 9 are a result of employing regularization from (72) [29]. If we use the same regularization as in [12,21,40], the Page curve will not exhibit negative values. It should be emphasized that we are more focused on the temporal behavioral changes of the radiative entanglement entropy rather than specific values.

Apart from the entanglement velocity v, the initial area difference $\Delta\mathcal{A}(0)$ between the HM surfaces and island

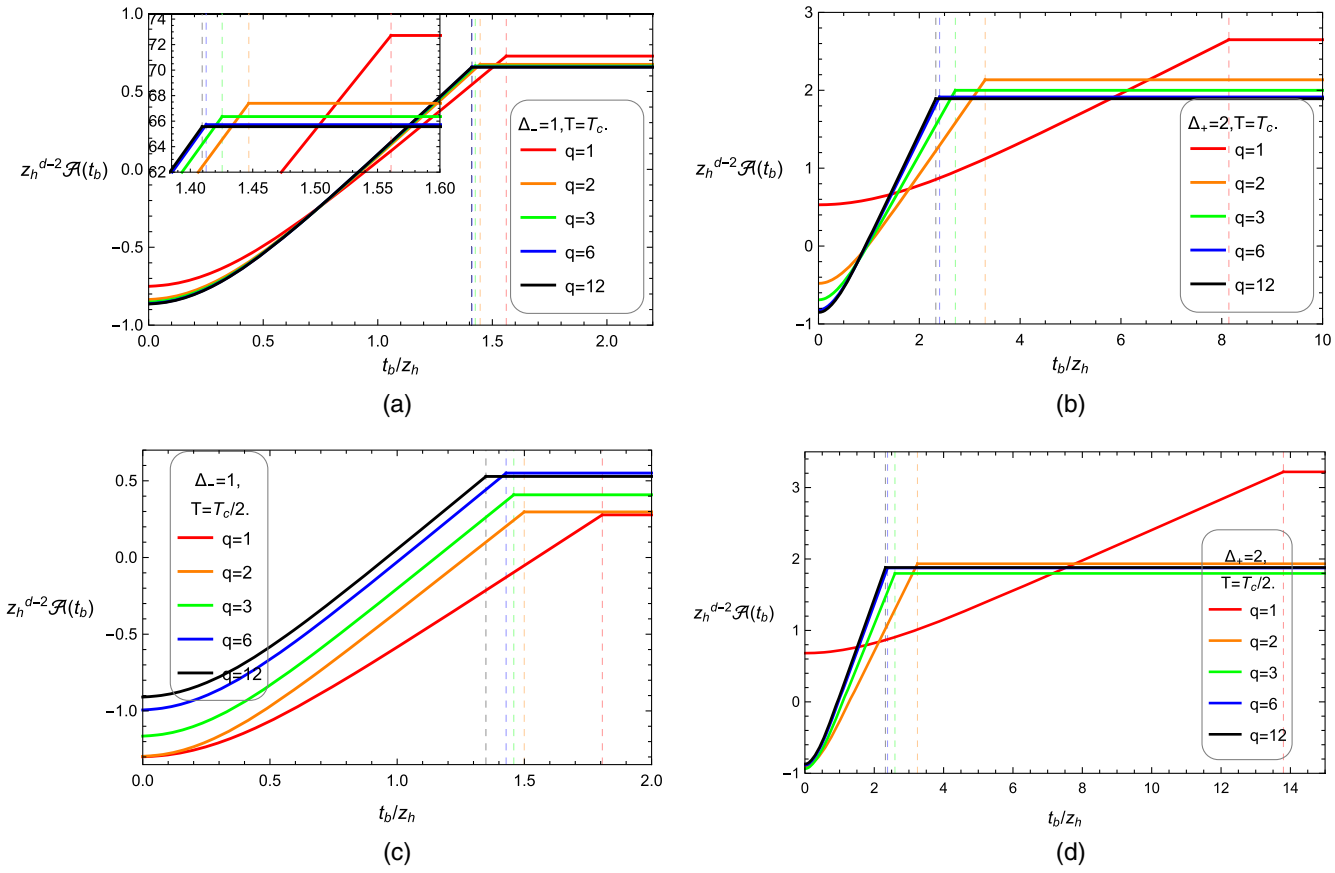

FIG. 9. The Page curves for two conformal dimension (a),(c) $\Delta_- = 1$; (b),(d) $\Delta_+ = 2$ at the critical temperature (a),(b) $T = T_c$ and semi-critical temperature (c),(d) $T = T_c/2$ are presented in terms of the area $\mathcal{A}$ and boundary time t_b in units of z_h.

surfaces also affects the Page time. It raises the question of which has a more significant impact on the Page time. We employ a method similar to that in [29] to provide a brief discussion on this issue. Without loss of generality, let us consider the case where the charge ($q = 1$) and conformal dimension ($\Delta_- = 1$), which corresponds to the red solid line in Figs. 9(a) and 9(c). According to our numerical calculations, the entanglement velocity, the initial area difference, and the Page time at the critical temperature and semicritical temperature are

$$v|_{T=T_c} \approx 0.61155, \qquad v|_{T=\frac{T_c}{2}} \approx 0.539485, \tag{74}$$

$$\Delta\mathcal{A}(0)|_{T=T_c} \approx 1.474922, \qquad \Delta\mathcal{A}(0)|_{T=\frac{T_c}{2}} \approx 1.576144, \tag{75}$$

$$\left.\frac{t_p}{z_h}\right|_{T=T_c} \approx 1.56084, \qquad \left.\frac{t_p}{z_h}\right|_{T=\frac{T_c}{2}} \approx 1.806469. \tag{76}$$

In the assumption that the evolution of the HM surface is always linear, the Page time can be approximated using (58) in the following manner

$$t_p \approx \frac{\Delta\mathcal{A}(0)}{2v}, \tag{77}$$

then we can get the "first-order" variation in the Page time δt_p

$$\delta t_p \approx \frac{\delta(\Delta\mathcal{A}(0))}{2v} - \frac{\Delta\mathcal{A}(0)}{2v^2}\delta v. \tag{78}$$

We calculate the average values of $\Delta\mathcal{A}(0)$ and v by using the results (74) and (75), and then substitute them into the formula above to obtain[5]

$$\delta t_p \approx 0.0879399 + 0.165962 = 0.253902 \approx 0.245629. \tag{79}$$

The right side of the last approximately equal sign in the above expression is from the numerical result (76) of the Page time. Using the same approximate calculations,

[5]Express the above result as the sum of two terms and set $z_h = 1$.

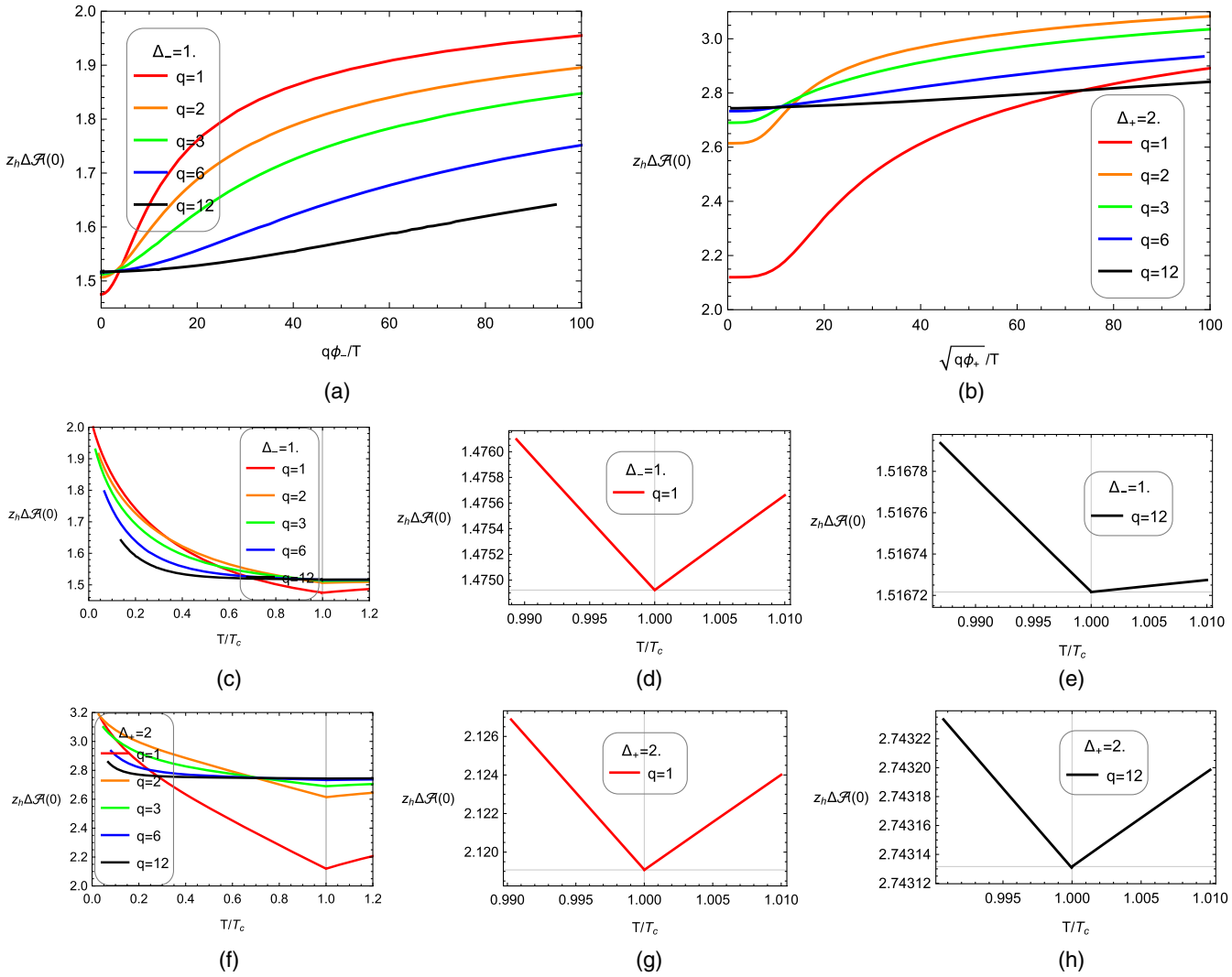

FIG. 10. The initial area differences $\Delta\mathcal{A}(0)$ are plotted as the function of deformations (a) $q\phi_-/T$; (b) $\sqrt{q\phi_+}/T$. (c),(f) represent the variation of initial area difference $\Delta\mathcal{A}(0)$ with the temperature T/T_c for the different charges, while (d),(e),(g),(h) represent the situation near the critical temperature for the charge $(q = 1)$ and $(q = 12)$.

we can obtain the change in the Page time from the critical temperature to the semi-critical temperature for the case of charge $(q = 1)$ and conformal dimension $\Delta_+ = 2$,

$$\delta t_p \approx 1.55988 + 3.55321 = 5.11308 \approx 5.65798. \quad (80)$$

Even these calculation are not always accurate.[6] Still, it is sufficient to demonstrate that the contribution from the entanglement velocity v has a more significant impact on the Page time than the contribution from the initial area difference $\Delta\mathcal{A}(0)$, which further indicates that the back-reaction from the interior of the black hole has a more significant influence on the Page time than the backreaction from the exterior of the black hole. Interestingly, our results are exactly opposite to the findings regarding neutral scalar deformations in [29].

In Figs. 10 and 11, we provide the initial area difference and Page time as a function of bath deformation and temperature, respectively. We found that the initial area difference increases with increasing scalar deformation (decreasing temperature). Since greater deformation leads to a smaller Page point, keeping the value of $x_{\mathcal{R}}$ constant results in an increase in the initial area difference as the Page point becomes smaller. The similar curves between Figs. 8(d), 8(e) and 10(a), 10(b) (except one increasing and one decreasing) indicates a connection between the initial area difference and the Page point. We also observe that the critical initial area difference (when $q\phi_\pm = 0$) increases with an increase in the charge. This is because at the critical temperature, the Page point decreases as the

[6]For example, in the case of $q = 12$, this kind of approximate calculation yields results that differ significantly from the numerical results.

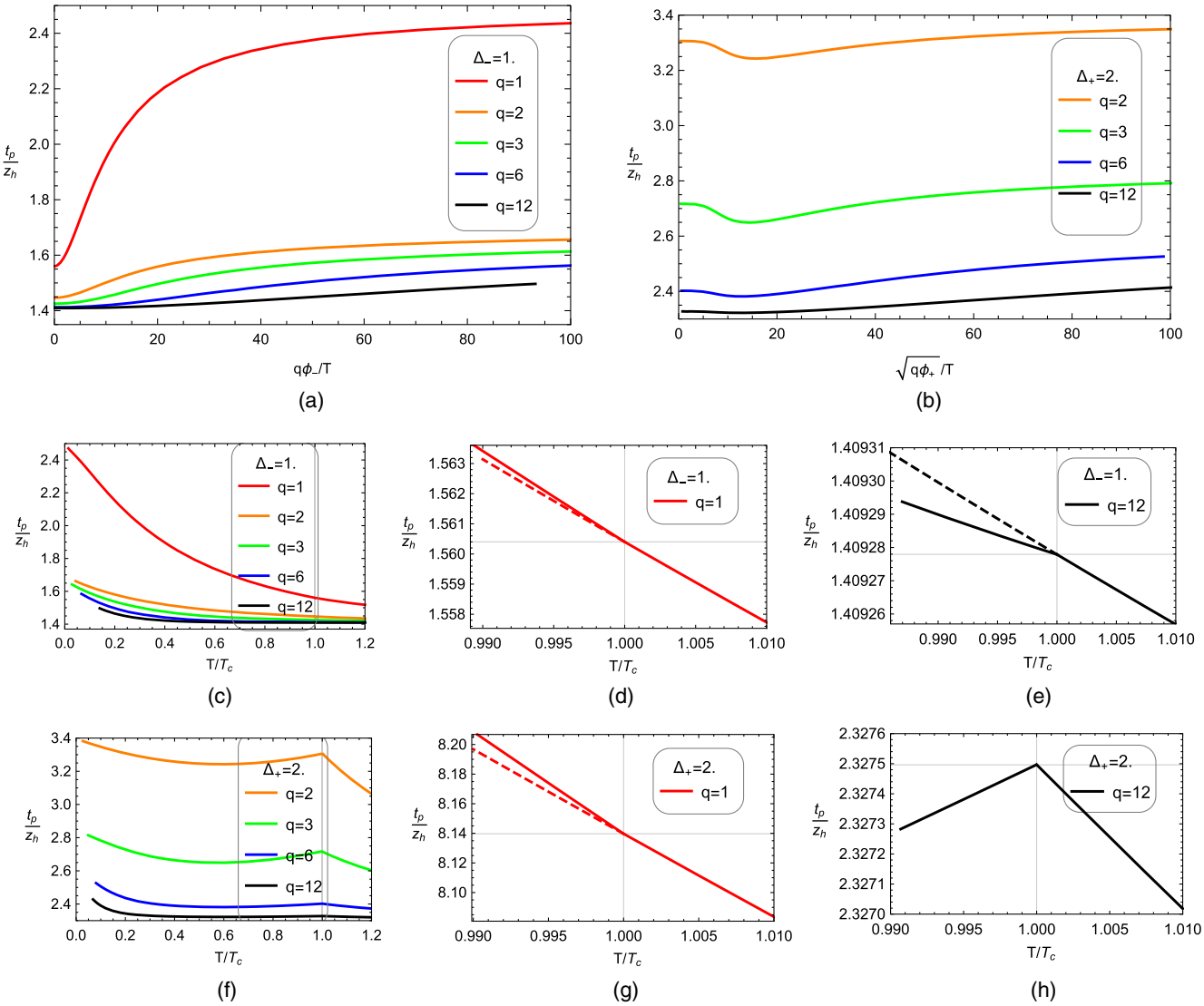

FIG. 11. The Page times t_p are plotted as functions of the deformation (a) $q\phi_-/T$; (b) $\sqrt{q\phi_+}/T$. (c),(f) represent the variation in Page time t_p with the temperature T/T_c for different charges, while (d),(e),(g),(h) represent the situation near the critical temperature for the charge $q = 1$ and $q = 12$. Since the page time for the case ($\Delta_+ = 2$, $q = 1$) is too big compared with other cases, it is not convenient to be presented in the same figure (b). The dashed line in the (d),(g) represents the Page time corresponding to the normal phase extending below the critical temperature.

charge increases, as seen the Fig. 8(c). Due to the clear discontinuity in the slope of the initial area difference at the critical temperature, the initial area difference can serve as a valuable probe for superconducting phase transitions.

From the curves of all charges in Fig. 11(a) and the curves for charge ($q = 1$) in Fig. 11(b), it is not difficult to observe that the Page time increases with the scalar deformation. However, for the cases of the conformal dimension ($\Delta_+ = 2$) and charges ($q = 2, 3, 6$, and 12) in Fig. 11(b), the Page time initially decreases and then increases with deformation. This behavior is related to the corresponding behavior of the entanglement velocity which initially increases and then decreases with deformation in Fig. 7(b). This further indirectly validates our earlier conclusion that the entanglement velocity has a more significant impact on the Page time than the initial area difference. In other words, the internal backreaction has a more significant impact on the Page time than the external backreaction. From Figs. 11(d), 11(e), 11(g), and 11(h), we can observe that the slope of the Page time with respect to temperature is discontinuous at the critical temperature. This indicates that the Page time can serve as a valuable probe for superconducting phase transitions.

It is worth noting that in all the calculations above, we have fixed the value of $x_{\mathcal{R}}$ to be twice the critical Page point (73). In fact, whether internal or external backreaction has a greater impact on the Page time also depends on the value of $x_{\mathcal{R}}$, which is related to the radiation region $\mathcal{R}$ [29].

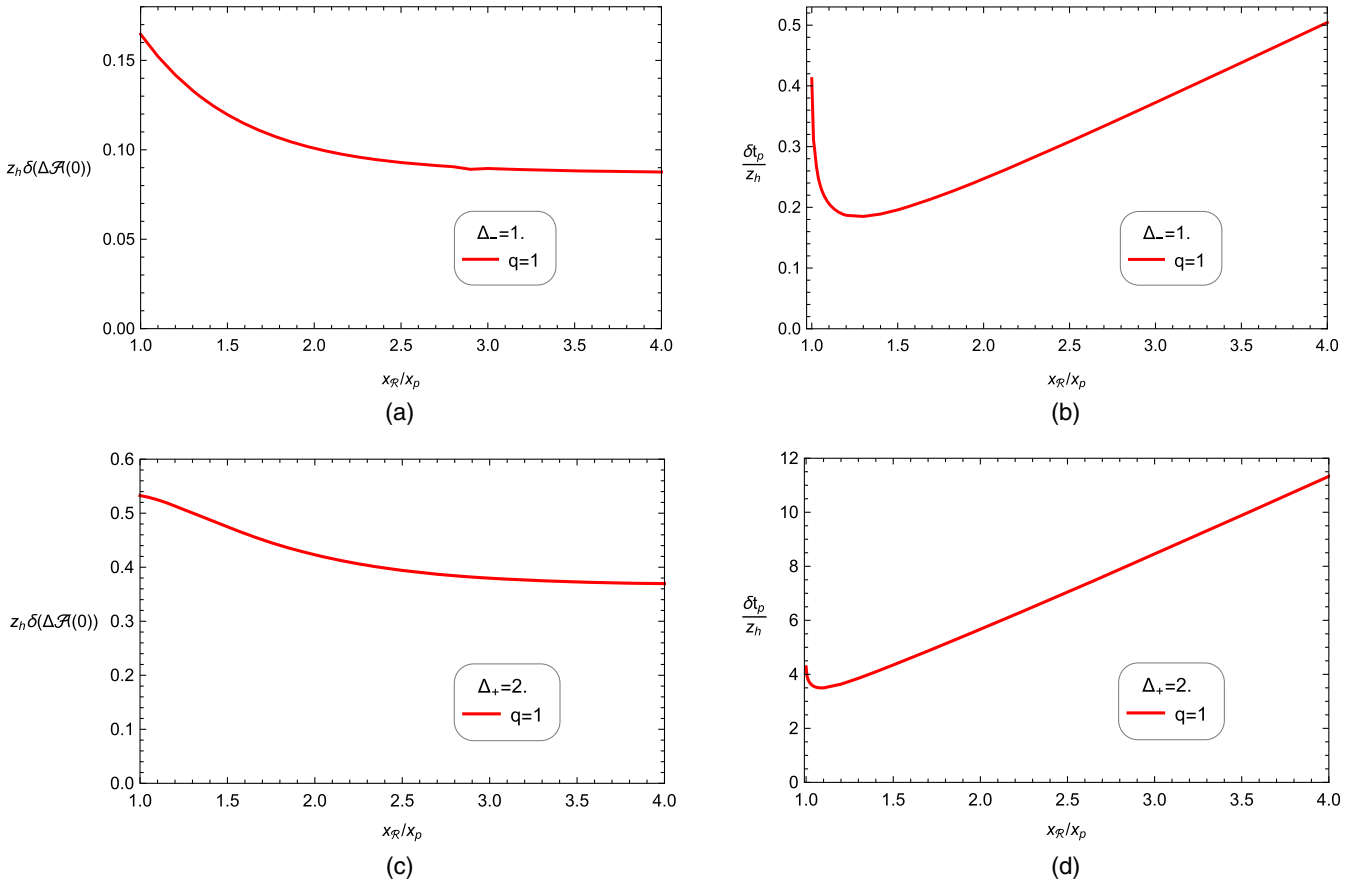

FIG. 12. The variations in the initial area difference and the Page time between the critical temperature and the semicritical temperature are presented in terms of radiation $x_\mathcal{R}$ region in units of z_h.

To study this issue, we consider the variation in the initial area difference $\delta(\Delta\mathcal{A}(0))$ and the variation in the Page time δt_p between the critical temperature $T = T_c$ and the semicritical temperature $T = T_c/2$. Without loss of generality, we only consider the case of charge ($q = 1$), while keeping the other constants set as $d = 3$ and $m^2 = -2$. More specifically, we consider the following variation in the initial area difference and the variation in the Page time:

$$\delta(\Delta\mathcal{A}(0)) = \Delta\mathcal{A}(0)|_{T=T_c/2} - \Delta\mathcal{A}(0)|_{T=T_c}, \quad (81)$$

$$\delta t_p = t_p|_{T=T_c/2} - t_p|_{T=T_c}. \quad (82)$$

In Fig. 12, the variations in the initial area difference and the Page time are presented in terms of $x_\mathcal{R}$. From Fig. 12, it is evident that the variation in the initial area difference decreases as $x_\mathcal{R}$ increases. However, according to (78), the variation in Page time should also decrease continuously. In fact, the variation in Page time initially decreases with increasing $x_\mathcal{R}$ and then linearly increases. Hence, we can conclude that the initial decrease (when $x_\mathcal{R} \approx x_p$) in the variation of the Page time is contributed by the variation in the initial area difference. The subsequent linear increase (when $x_\mathcal{R} \gg x_p$) in the variation of the Page time is attributed to the second term in the expression (78), which is the contribution of the variation in the entanglement velocity. In other words, when $x_\mathcal{R} \approx x_p$, the external backreaction has a more significant impact on the Page time. When $x_\mathcal{R} \gg x_p$, the internal backreaction has a more substantial influence on the Page time. Our conclusion aligns perfectly with the findings regarding neutral scalar deformations [29]. Finally, it is worth mentioning that in our model, $x_\mathcal{R} = 2x_p$ falls within the $x_\mathcal{R} \gg x_p$ region, which is why the previous calculations conclude that the entanglement velocity has a more significant impact on Page time than the initial area difference. However, for the case of neutral scalar deformations [29], $x_\mathcal{R} = 2x_p$ falls within the $x_\mathcal{R} \approx x_p$ region, and that is why the conclusion is drawn that external backreaction has a more significant influence on Page time than internal backreaction.

VI. CONCLUSIONS AND OUTLOOK

In this paper, we employ a dual holographic model that deforms the conformal bath with a charged scalar field to investigate how the bath deformation affects the Page curve. Unlike the neutral deformation, due to the

spontaneous symmetry breaking of the U(1) gauge field, it induces a second-order phase transition of the charged scalar field, known as the holographic superconductors.

We have discovered that the characteristic parameters of the Page curve, such as entanglement velocity, initial area difference, and Page time, can be used as suitable probes to detect the superconducting phase transitions. Specifically, the entanglement velocity can probe both the Kasner flows and Josephson oscillations.

When keeping $x_{\mathcal{R}}$ fixed, we find that the growth behavior of the Page time with an increasing deformation parameter (or decreasing temperature) is related to the conformal dimension $\Delta_{\pm}$. Specifically, the Page time monotonically increases with an increasing deformation for $\Delta_- = 1$ (corresponding to the "Neumann" ($\Delta = \Delta_-$) quantization). However, for $\Delta_+ = 2$ (corresponding to the "Dirichlet" ($\Delta = \Delta_+$) quantization), and charges ($q = 2, 3, 6$, and 12), the Page time initially decreases and then increases with an increasing deformation (or a decreasing temperature). The behavior of the Page time decreasing as the temperature lowers is closely related to the corresponding behavior of the entanglement velocity. In the case of charge ($q = 1$), the behavior of the Page time is similar to the former. For Δ_+, the Page time is generally larger than the Page time for Δ_-. Furthermore, a larger charge leads to a smaller Page time for the same conformal dimension and fixed temperature.

When $x_{\mathcal{R}}$ is fixed at twice the critical Page point $x_{\mathcal{R}} = 2x_p$, changes in the entanglement velocity (the internal backreaction) has a more significant influence on the Page time compared to changes in the initial area difference (the external backreaction). By varying the value of $x_{\mathcal{R}}$, we further discover that when $x_{\mathcal{R}} \gg x_p$, meaning the black hole has more boundary degrees of freedom, the internal backreaction has a more significant effect on the Page time compared to the external backreaction, which is consistent with results for the case of neutral scalar deformations [29].

In recent years, an information-theoretic quantity known as computational complexity has been related to the gravitational concept within the context of AdS/CFT duality [131–135]. Interestingly, the holographic complexity has also received extensive research in the holographic superconducting model [76,83,136–140]. Inspired by previous research in the holographic complexity with the doubly holographic model [24,24,129,141,142]. In the future, we are interested in exploring the holographic complexity of the holographic superconducting models but with a doubly holographic setup.

ACKNOWLEDGMENTS

Y. C. X. would like to thank Professor Tao-Tao Qiu of Huazhong University of Science and Technology for his helpful discussions and suggestions. Y. C. X. also thanks Professor Rong-Xin Miao of Sun Yat-Sen University for his helpful discussions and suggestions about the doubly holographic setup. This work was supported by the National Natural Science Foundation of China under Grants No. 11653002 and No. 11875141. Dr. Jia-Ming Shi of Hangzhou Institute for Advanced Study also provided financial support for this work. Grateful thanks to Dr. Shi for the support of the Fundamental Research Funds for Central Universities (Innovation Funded Projects) under Grants No. 2020CXZZ105.

APPENDIX

In this appendix, following the steps of Ref. [40] and the NBCs of the gauge field with topological terms, we will demonstrate that for a system with a finite charge density ρ but without an external magnetic field B, both the tension of the brane and topological terms should vanish. First, we consider the following NBC as in [111,112],

$$\frac{1}{2} * F + \left(\frac{\Theta}{8\pi^2} + \frac{k}{4\pi}\right) F|_Q = 0, \tag{A1}$$

where $*$ is the epsilon symbol in AdS_4, Θ and k originates from the topological term and Chern-Simons term on the brane. Substituting $*F = \frac{1}{2} * F_{\mu\nu} dx^\mu \wedge dx^\nu$ and $*F_{\mu\nu} = \frac{1}{2}\epsilon_{\mu\nu\rho\sigma}F^{\rho\sigma}$ into NBC (A1), the above equation can be rewritten as the following form in the component notation

$$\frac{1}{4}\sqrt{-g}\epsilon_{\mu\nu\rho\sigma}F^{\rho\sigma} + \left(\frac{\Theta}{8\pi^2} + \frac{k}{4\pi}\right) F_{\mu\nu}|_Q = 0. \tag{A2}$$

To restrict the bulk equation on Q, we may project it on a 3-form orthogonal to the normal vector n^μ and obtain

$$-\frac{1}{2}\sqrt{-g}n_\nu F^{\nu\mu} + \frac{1}{2}\left(\frac{\Theta}{8\pi^2} + \frac{k}{4\pi}\right) n_\nu \epsilon^{\nu\mu\rho\sigma} F_{\rho\sigma} = 0. \tag{A3}$$

To find the solution of the boundary equation, we define an outward unit vector normal to Q

$$(n^t, n^x, n^y, n^z) = \frac{z}{L}\left(0, \frac{1}{\sqrt{1 + f(z)x_1'(z)^2}}, 0, -\frac{f(z)x_1'(z)}{\sqrt{1 + f(z)x_1'(z)^2}}\right). \tag{A4}$$

Using the position of the Planck brane $x_1 = z\cot(\theta)$ and pure AdS_4 metric $f(z) = 1$, the unit vector normal can be rewritten as $(n^t, n^x, n^y, n^z) = \frac{z}{L}[0, \sin(\theta), 0, -\cos(\theta)]$. In this appendix, we make the following simple ansatz for the gauge fields

$$A_t = \mu - \rho z, \qquad A_x = -By, \qquad A_{y,z} = 0. \tag{A5}$$

Then, Eq. (A3) gives two equations as

$$\begin{aligned} \rho\cos(\theta) + c_{pb}B\cos(\theta) &= 0, \\ B\sin(\theta) - c_{pb}\rho\sin(\theta) &= 0, \end{aligned} \tag{A6}$$

where the constant c_{pb} was defined as $c_{pb} = \frac{\Theta}{4\pi^2} + \frac{k}{2\pi}$. When considering a system with a finite charge density

ρ but without an external magnetic field B, from the above equations in (A6), we can obtain

$$(\rho \neq 0, B = 0): \quad \theta = \frac{\pi}{2} \,\&\, c_{pb} = 0. \tag{A7}$$

In other words, both the tension of the brane and topological terms should vanish, as described in Ref. [40]. Since models involving Planck branes are bottom-up models which, in principle, could not have a proper UV completion, it is possible that the full-fledged string theory solution dual to a charged system in the AdS/BCFT or a doubly holographic setup does not look at all like a Planck brane model, and from the bottom up, it is shown in this constraint condition. Thus, from various points of view, considering tensionless branes is simple and practical.

[1] G. Penington, J. High Energy Phys. 09 (2020) 002.
[2] A. Almheiri, N. Engelhardt, D. Marolf, and H. Maxfield, J. High Energy Phys. 12 (2019) 063.
[3] A. Almheiri, R. Mahajan, and J. Maldacena, arXiv:1910.11077.
[4] A. Almheiri, R. Mahajan, J. Maldacena, and Y. Zhao, J. High Energy Phys. 03 (2020) 149.
[5] A. Almheiri, T. Hartman, J. Maldacena, E. Shaghoulian, and A. Tajdini, Rev. Mod. Phys. **93**, 035002 (2021).
[6] S. W. Hawking, Phys. Rev. D **14**, 2460 (1976).
[7] N. Engelhardt and A. C. Wall, J. High Energy Phys. 01 (2015) 073.
[8] D. N. Page, Phys. Rev. Lett. **71**, 3743 (1993).
[9] D. N. Page, J. Cosmol. Astropart. Phys. 09 (2013) 028.
[10] G. Penington, S. H. Shenker, D. Stanford, and Z. Yang, J. High Energy Phys. 03 (2022) 205.
[11] A. Almheiri, T. Hartman, J. Maldacena, E. Shaghoulian, and A. Tajdini, J. High Energy Phys. 05 (2020) 013.
[12] A. Almheiri, R. Mahajan, and J. E. Santos, SciPost Phys. **9**, 001 (2020).
[13] L. Randall and R. Sundrum, Phys. Rev. Lett. **83**, 4690 (1999).
[14] L. Randall and R. Sundrum, Phys. Rev. Lett. **83**, 3370 (1999).
[15] A. Karch and L. Randall, J. High Energy Phys. 05 (2001) 008.
[16] A. Karch and L. Randall, J. High Energy Phys. 06 (2001) 063.
[17] H. Geng and A. Karch, J. High Energy Phys. 09 (2020) 121.
[18] V. Chandrasekaran and M. Miyaji, Phys. Rev. D **102**, 086009 (2020).
[19] C. Krishnan, J. High Energy Phys. 01 (2021) 179.
[20] H. Z. Chen, Z. Fisher, J. Hernandez, R. C. Myers, and S.-M. Ruan, J. High Energy Phys. 01 (2021) 065.
[21] Y. Ling, Y. Liu, and Z.-Y. Xian, J. High Energy Phys. 03 (2021) 251.
[22] Y. Ling, P. Liu, Y. Liu, C. Niu, Z.-Y. Xian, and C.-Y. Zhang, J. High Energy Phys. 02 (2022) 037.
[23] H. Geng, A. Karch, C. Perez-Pardavila, S. Raju, L. Randall, M. Riojas, and S. Shashi, SciPost Phys. **10**, 103 (2021).
[24] A. Bhattacharya, A. Bhattacharyya, P. Nandy, and A. K. Patra, J. High Energy Phys. 05 (2021) 135.
[25] K. Ghosh and C. Krishnan, J. High Energy Phys. 08 (2021) 119.
[26] H. Geng, S. Lüst, R. K. Mishra, and D. Wakeham, J. High Energy Phys. 08 (2021) 003.
[27] C. F. Uhlemann, J. High Energy Phys. 08 (2021) 104.
[28] D. Neuenfeld, Classical Quantum Gravity **39**, 075009 (2022).
[29] E. Caceres, A. Kundu, A. K. Patra, and S. Shashi, SciPost Phys. Core **5**, 033 (2022).
[30] H. Omiya and Z. Wei, J. High Energy Phys. 07 (2022) 128.
[31] H. Geng, A. Karch, C. Perez-Pardavila, S. Raju, L. Randall, M. Riojas, and S. Shashi, J. High Energy Phys. 01 (2022) 182.
[32] P.-C. Sun, arXiv:2108.12557.
[33] C.-J. Chou, H. B. Lao, and Y. Yang, Phys. Rev. D **106**, 066008 (2022).
[34] H. Geng, A. Karch, C. Perez-Pardavila, S. Raju, L. Randall, M. Riojas, and S. Shashi, J. High Energy Phys. 153 (2022) 05.
[35] Q.-L. Hu, D. Li, R.-X. Miao, and Y.-Q. Zeng, J. High Energy Phys. 09 (2022) 037.
[36] T. Anous, M. Meineri, P. Pelliconi, and J. Sonner, SciPost Phys. **13**, 075 (2022).
[37] S. Demulder, A. Gnecchi, I. Lavdas, and D. Lust, J. High Energy Phys. 02 (2023) 016.
[38] D. Basu, Q. Wen, and S. Zhou, arXiv:2211.17004.
[39] A. Karch, C. Perez-Pardavila, and M. Riojas, J. High Energy Phys. 05 (2023) 195.
[40] H.-S. Jeong, K.-Y. Kim, and Y.-W. Sun, Phys. Rev. D **108**, 126016 (2023).
[41] J.-C. Chang, S. He, Y.-X. Liu, and L. Zhao, J. High Energy Phys. 11 (2023) 006.
[42] D. Basu, H. Parihar, V. Raj, and G. Sengupta, Phys. Rev. D **108**, 106005 (2023).
[43] M. Afrasiar, D. Basu, A. Chandra, V. Raj, and G. Sengupta, J. High Energy Phys. 11 (2023) 192.
[44] C.-J. Chou, H. B. Lao, and Y. Yang, J. High Energy Phys. 05 (2024) 342.
[45] S. Ryu and T. Takayanagi, Phys. Rev. Lett. **96**, 181602 (2006).
[46] V. E. Hubeny, M. Rangamani, and T. Takayanagi, J. High Energy Phys. 07 (2007) 062.
[47] T. Hartman and J. Maldacena, J. High Energy Phys. 05 (2013) 014.

[48] K. Hashimoto, N. Iizuka, and Y. Matsuo, J. High Energy Phys. 06 (2020) 085.
[49] M. Alishahiha, A. Faraji Astaneh, and A. Naseh, J. High Energy Phys. 02 (2021) 035.
[50] H. Z. Chen, R. C. Myers, D. Neuenfeld, I. A. Reyes, and J. Sandor, J. High Energy Phys. 12 (2020) 025.
[51] M.-H. Yu and X.-H. Ge, Eur. Phys. J. C **82**, 14 (2022).
[52] M.-H. Yu, C.-Y. Lu, X.-H. Ge, and S.-J. Sin, Phys. Rev. D **105**, 066009 (2022).
[53] M.-H. Yu and X.-H. Ge, Phys. Rev. D **107**, 066020 (2023).
[54] W.-C. Gan, D.-H. Du, and F.-W. Shu, J. High Energy Phys. 07 (2022) 020.
[55] D.-H. Du, W.-C. Gan, F.-W. Shu, and J.-R. Sun, Phys. Rev. D **107**, 026005 (2023).
[56] C.-Z. Guo, W.-C. Gan, and F.-W. Shu, J. High Energy Phys. 05 (2023) 042.
[57] S. He, Y. Sun, L. Zhao, and Y.-X. Zhang, J. High Energy Phys. 05 (2022) 047.
[58] S. A. Hosseini Mansoori, O. Luongo, S. Mancini, M. Mirjalali, M. Rafiee, and A. Tavanfar, Phys. Rev. D **106**, 126018 (2022).
[59] X. Wang, R. Li, and J. Wang, J. High Energy Phys. 04 (2021) 103.
[60] G. Yadav, Eur. Phys. J. C **82**, 904 (2022).
[61] V. Balasubramanian and P. Kraus, Phys. Rev. Lett. **83**, 3605 (1999).
[62] J. de Boer, Fortschr. Phys. **49**, 339 (2001).
[63] M. Bianchi, D. Z. Freedman, and K. Skenderis, Nucl. Phys. **B631**, 159 (2002).
[64] M. Fukuma, S. Matsuura, and T. Sakai, Prog. Theor. Phys. **109**, 489 (2003).
[65] S. S. Gubser, Phys. Rev. D **78**, 065034 (2008).
[66] S. A. Hartnoll, C. P. Herzog, and G. T. Horowitz, Phys. Rev. Lett. **101**, 031601 (2008).
[67] S. A. Hartnoll, C. P. Herzog, and G. T. Horowitz, J. High Energy Phys. 12 (2008) 015.
[68] T. Albash and C. V. Johnson, J. High Energy Phys. 05 (2012) 079.
[69] A. Dutta and S. K. Modak, J. High Energy Phys. 01 (2014) 136.
[70] X.-M. Kuang, E. Papantonopoulos, and B. Wang, J. High Energy Phys. 05 (2014) 130.
[71] W. Yao and J. Jing, Nucl. Phys. **B889**, 109 (2014).
[72] A. Dey, S. Mahapatra, and T. Sarkar, J. High Energy Phys. 12 (2014) 135.
[73] X. Bai, B.-H. Lee, L. Li, J.-R. Sun, and H.-Q. Zhang, J. High Energy Phys. 04 (2015) 066.
[74] A. M. García-García and A. Romero-Bermúdez, J. High Energy Phys. 09 (2015) 033.
[75] H.-S. Jeong, K.-Y. Kim, and Y.-W. Sun, J. High Energy Phys. 06 (2022) 078.
[76] D. Wang, X. Qiao, M. Wang, Q. Pan, C. Lai, and J. Jing, Nucl. Phys. **B991**, 116223 (2023).
[77] C. Lai and Q. Pan, Eur. Phys. J. C **83**, 583 (2023).
[78] R.-G. Cai, S. He, L. Li, and Y.-L. Zhang, J. High Energy Phys. 07 (2012) 027.
[79] R. E. Arias and I. S. Landea, J. High Energy Phys. 01 (2013) 157.
[80] L.-F. Li, R.-G. Cai, L. Li, and C. Shen, Nucl. Phys. **B894**, 15 (2015).
[81] S. R. Das, M. Fujita, and B. S. Kim, J. High Energy Phys. 09 (2017) 016.
[82] Z. Yang, F.-J. Cheng, C. Niu, C.-Y. Zhang, and P. Liu, J. High Energy Phys. 04 (2023) 110.
[83] Y. Xu, Y. Shi, D. Wang, and Q. Pan, Eur. Phys. J. C **83**, 202 (2023).
[84] R.-G. Cai, S. He, L. Li, and Y.-L. Zhang, J. High Energy Phys. 07 (2012) 088.
[85] R.-G. Cai, S. He, L. Li, and L.-F. Li, J. High Energy Phys. 10 (2012) 107.
[86] W. Yao and J. Jing, J. High Energy Phys. 05 (2014) 058.
[87] Y. Peng and Q. Pan, J. High Energy Phys. 06 (2014) 011.
[88] Y. Peng and G. Liu, Phys. Lett. B **767**, 330 (2017).
[89] W. Yao, C. Yang, and J. Jing, Eur. Phys. J. C **78**, 353 (2018).
[90] W. Yao, Q. Yang, X. Liu, and J. Jing, Eur. Phys. J. C **81**, 355 (2021).
[91] R.-G. Cai, L. Li, L.-F. Li, and R.-K. Su, J. High Energy Phys. 06 (2013) 063.
[92] E. Verheijden and E. Verlinde, J. High Energy Phys. 11 (2021) 092.
[93] H. Geng, Y. Nomura, and H.-Y. Sun, Phys. Rev. D **103**, 126004 (2021).
[94] D. Li and R.-X. Miao, J. High Energy Phys. 06 (2023) 056.
[95] A. Bhattacharya, A. Bhattacharyya, and A. K. Patra, J. High Energy Phys. 07 (2023) 060.
[96] Z. Li and Z. Hong, arXiv:2308.15861.
[97] R.-X. Miao, J. High Energy Phys. 06 (2024) 043.
[98] Z.-Q. Cui, Y. Guo, and R.-X. Miao, J. High Energy Phys. 03 (2024) 158.
[99] Y. Liu, S.-K. Jian, Y. Ling, and Z.-Y. Xian, arXiv:2401.04706.
[100] Y. Guo and R.-X. Miao, Eur. Phys. J. C **83**, 847 (2023).
[101] R.-X. Miao, Eur. Phys. J. C **84**, 123 (2024).
[102] A. Frenkel, S. A. Hartnoll, J. Kruthoff, and Z. D. Shi, J. High Energy Phys. 08 (2020) 003.
[103] Y.-Q. Wang, Y. Song, Q. Xiang, S.-W. Wei, T. Zhu, and Y.-X. Liu, arXiv:2009.06277.
[104] S. A. Hartnoll, G. T. Horowitz, J. Kruthoff, and J. E. Santos, J. High Energy Phys. 10 (2020) 102.
[105] S. A. Hartnoll, G. T. Horowitz, J. Kruthoff, and J. E. Santos, SciPost Phys. **10**, 009 (2021).
[106] R.-G. Cai, L. Li, and R.-Q. Yang, J. High Energy Phys. 03 (2021) 263.
[107] L. Sword and D. Vegh, J. High Energy Phys. 04 (2022) 135.
[108] N. Grandi and I. Salazar Landea, J. High Energy Phys. 05 (2021) 152.
[109] Y.-S. An, L. Li, and F.-G. Yang, Phys. Rev. D **104**, 024040 (2021).
[110] D. O. Devecioglu and M.-I. Park, Eur. Phys. J. C **84**, 168 (2024).
[111] M. Fujita, M. Kaminski, and A. Karch, J. High Energy Phys. 07 (2012) 150.
[112] D. Melnikov, E. Orazi, and P. Sodano, J. High Energy Phys. 05 (2013) 116.
[113] F. F. Santos, E. F. Capossoli, and H. Boschi-Filho, Phys. Rev. D **104**, 066014 (2021).
[114] F. F. Santos, M. Bravo-Gaete, O. Sokoliuk, and A. Baransky, Fortschr. Phys. **71**, 2300008 (2023).

[115] F. F. Santos, M. Bravo-Gaete, M. M. Ferreira, and R. Casana, arXiv:2310.17092.
[116] C.-S. Chu and R.-X. Miao, J. High Energy Phys. 07 (2018) 005.
[117] R.-X. Miao, J. High Energy Phys. 02 (2019) 025.
[118] C.-S. Chu and R.-X. Miao, J. High Energy Phys. 08 (2020) 134.
[119] S. A. Hartnoll, Classical Quantum Gravity **26**, 224002 (2009).
[120] C. P. Herzog, J. Phys. A **42**, 343001 (2009).
[121] G. T. Horowitz, Lect. Notes Phys. **828**, 313 (2011).
[122] G. T. Horowitz and M. M. Roberts, Phys. Rev. D **78**, 126008 (2008).
[123] R.-G. Cai, L. Li, L.-F. Li, and R.-Q. Yang, Sci. China Phys. Mech. Astron. **58**, 060401 (2015).
[124] M. Mirjalali, S. A. Hosseini Mansoori, L. Shahkarami, and M. Rafiee, J. High Energy Phys. 09 (2022) 222.
[125] E. Kasner, Am. J. Math. **43**, 217 (1921).
[126] E. Kasner, Trans. Am. Math. Soc. **27**, 155 (1925).
[127] V. A. Belinski and I. M. Khalatnikov, Sov. Phys. JETP **36**, 591 (1973).
[128] D. Carmi, S. Chapman, H. Marrochio, R. C. Myers, and S. Sugishita, J. High Energy Phys. 11 (2017) 188.
[129] A. Bhattacharya, A. Bhattacharyya, P. Nandy, and A. K. Patra, Phys. Rev. D **105**, 066019 (2022).
[130] S. A. H. Mansoori, L. Li, M. Rafiee, and M. Baggioli, J. High Energy Phys. 10 (2021) 098.
[131] L. Susskind, Fortschr. Phys. **64**, 24 (2016); **64**, 44(E) (2016).
[132] D. Stanford and L. Susskind, Phys. Rev. D **90**, 126007 (2014).
[133] A. R. Brown, D. A. Roberts, L. Susskind, B. Swingle, and Y. Zhao, Phys. Rev. Lett. **116**, 191301 (2016).
[134] A. R. Brown, D. A. Roberts, L. Susskind, B. Swingle, and Y. Zhao, Phys. Rev. D **93**, 086006 (2016).
[135] M. Alishahiha, Phys. Rev. D **92**, 126009 (2015).
[136] M. Kord Zangeneh, Y. C. Ong, and B. Wang, Phys. Lett. B **771**, 235 (2017).
[137] M. Fujita, Prog. Theor. Exp. Phys. **2019**, 063B04 (2019).
[138] R.-Q. Yang, H.-S. Jeong, C. Niu, and K.-Y. Kim, J. High Energy Phys. 04 (2019) 146.
[139] Y.-S. An, L. Li, F.-G. Yang, and R.-Q. Yang, J. High Energy Phys. 08 (2022) 133.
[140] R. Auzzi, S. Bolognesi, E. Rabinovici, F. I. Schaposnik Massolo, and G. Tallarita, J. High Energy Phys. 08 (2022) 235.
[141] A. Bhattacharya, A. Chanda, S. Maulik, C. Northe, and S. Roy, J. High Energy Phys. 02 (2021) 152.
[142] J. Hernandez, R. C. Myers, and S.-M. Ruan, J. High Energy Phys. 02 (2021) 173.